

## RESEARCH ARTICLE

# Observed rainfall asymmetry of tropical cyclone in the process of making landfall in Guangdong, south China

Guanhuan Wen<sup>1</sup>  | Gang Huang<sup>2,3</sup> | Huijun Huang<sup>1</sup> | Chunxia Liu<sup>1</sup> | Xueyan Bi<sup>1</sup><sup>1</sup>Guangzhou Institute of Tropical and Marine Meteorology, China Meteorological Administration, Guangzhou, China<sup>2</sup>Institute of Atmospheric Physics, Chinese Academy of Sciences, Beijing, China<sup>3</sup>University of Chinese Academy of Sciences, Beijing, China**Correspondence**

Guanhuan Wen

Guangzhou Institute of Tropical and Marine Meteorology, China Meteorological Administration, Guangzhou 510080, China.  
Email: ghwen@grmc.gov.cn

Gang Huang

Institute of Atmospheric Physics, Chinese Academy of Sciences, Beijing 100029, China.  
Email: hg@mail.iap.ac.cn**Funding information**

Natural Science Foundation of Guangdong Province, Grant/Award Number: 2016A030310009; National Basic Research Program of China, Grant/Award Number: 2015CB452802; National Natural Science Foundation of China, Grant/Award Numbers: 41425019, 41475061, 41475102, 41675019, 41675021; Scientific and Technological Research Project of Guangdong Meteorological Service, Grant/Award Number: GRMC2018M05; Guangzhou Science and Technology Plan Project, Grant/Award Number: 201510010218

This study investigates the rainfall asymmetry of tropical cyclones (TCs) in the process of making landfall in Guangdong (GD), south China, on the basis of satellite-based and reanalysis precipitation data. We mainly focus on TC rainfall asymmetry, its main influencing factor and its change in the process of landfall, and the difference between different El Niño–Southern Oscillation (ENSO) phases. The results reveal that vertical wind shear (VWS) is the dominant influencing factor of TC rainfall asymmetry in GD. The rainfall maximum is located in downshear left of VWS. The TC rainfall asymmetry has little change in the process of making landfall, though the rain rate decreases. Both the phase and amplitude of TC rainfall asymmetry have no significant change from 24 hr prior to landfall to 12 hr after landfall. The rainfall maximum steadily lies in downshear left. The amplitude of rainfall asymmetry is about 50%, suggesting that the asymmetric rainfall is about half of the axisymmetric rainfall. There is no obvious difference in TC rainfall asymmetry between El Niño, La Niña, and neutral years.

**KEYWORDS**

rainfall asymmetry, TRMM, tropical cyclone, vertical wind shear

## 1 | INTRODUCTION

A tropical cyclone (TC) is a rotating, organized system of clouds and thunderstorms that originates over tropical or subtropical ocean surface. There are about 80 TC geneses on average over global ocean annually (Emanuel, 2003). Some of the TCs would make landfall before dissipating. TCs can cause tremendous damages and large losses in coastal areas when they make landfall. One of the disaster-causing factors for landfalling TCs is heavy rainfall. TCs often bring about extreme rainfall. A large portion of extreme rainfall is contributed by TCs along coastal areas (Khouakhi *et al.*, 2016; Zhang *et al.*, 2017; Rios Gaona *et al.*, 2018; Zhang *et al.*,

2018). Chang *et al.* (2012) found that 50–70% of extreme rainfall along the southeastern coast of China was associated with TCs. Numbers of extreme rainfall events are related to landfalling TCs (Yu *et al.*, 2008; Chen *et al.*, 2010a; Dong *et al.*, 2013). The highest 24-hr rainfall record in China, which is 1748.5 mm observed at Ali Mountain, is associated with Super Typhoon Herb (9602) when it landed in Taiwan Island on July 31, 1996 (Chen *et al.*, 2010b). Extreme TC rainfall tends to result in widespread inland flood and other secondary disasters such as mudslides, causing huge losses in property and human lives. For example, the strongest rainfall event on mainland China occurred at Linzhuang of Henan province in August 1975 when Typhoon Nina (7503)

made landfall in China and moved inland. The 24-hr rainfall amount is up to 1,062 mm. This extreme rainfall event caused severe floods and killed tens of thousands of people (Chen *et al.*, 2010b). Therefore, investigation of TC rainfall is very important and necessary for the society and economy.

The spatial distribution of TC rainfall determines the region that experiences more rainfall or extreme rainfall. An adequate understanding of the rainfall distribution of land-falling TC is crucial in rainfall forecast and disaster mitigation (Chan *et al.*, 2001; Chan, 2008; Zhang *et al.*, 2010; Li *et al.*, 2013; Li *et al.*, 2015; Zhu *et al.*, 2015; Zhang *et al.*, 2016; Emanuel and Zhang, 2017). Many observations (Chan *et al.*, 2004; Lonfat *et al.*, 2004; Chen *et al.*, 2006; Liu *et al.*, 2007; Yuan *et al.*, 2010; Xu *et al.*, 2014; Yu *et al.*, 2015) showed that TC rainfall has asymmetric distribution over the ocean and on land. The rainfall of TCs is generally not symmetrically distributed and is usually more pronounced in a certain position of TCs. Some early studies (Marks, 1985; Burpee and Black, 1989) found that TCs over the ocean have a precipitation maximum in the front quadrant (front-right or front-left) of the storm when they analysed the rainfall distribution of TC cases. Composite analysis based on large number of TCs also showed a front rainfall maximum in some studies (Rodgers *et al.*, 1994; Lonfat *et al.*, 2004). Lonfat *et al.* (2004) indicated that the maximum rainfall for the average of global TCs is located in the front quadrants, and the location of the maximum rainfall is in the front-left quadrant for tropical storms and in the front-right for hurricanes and typhoons. This kind of asymmetry is related to asymmetric boundary layer convergence caused by storm motion (Shapiro, 1983; Lonfat *et al.*, 2004). In addition, the right side of storm track favours more rainfall when a TC makes landfall (Tuleya and Kurihara, 1978; Jones, 1987; Chen *et al.*, 2010b). Chen *et al.* (2010b) found that the maximum rainfall rates in the inner eyewall, outer eyewall, and rainband regions occurred in the right quadrant relative to the storm track for Typhoon Saomai (0608) when it got close to land. As a TC approaches land, surface friction gradient between land and sea induces a frictional convergence to the right side of the storm motion in the Northern Hemisphere (Xu *et al.*, 2014). Recently, more and more studies (Corbosiero and Molinari, 2002; Chen *et al.*, 2006; Wingo and Cecil, 2009; Yuan *et al.*, 2010; Chen and Fang, 2012; Xu *et al.*, 2014; Yu *et al.*, 2015) indicated that TC rainfall asymmetry is more related to the environmental vertical wind shear (VWS). These studies showed that a maximum of convection and rain rate occurs in downshear or downshear left of VWS. Some studies (Xu *et al.*, 2014; Yu *et al.*, 2015) even pointed out that environmental VWS is the dominant factor that produces TC rainfall asymmetry comparing to other factors.

The El Niño–Southern Oscillation (ENSO) is a tropical atmosphere–ocean interaction that modifies the

thermodynamic and dynamic states that influence the weather and climate system (Bjerknes, 1969). The ENSO phenomenon plays an important role in modulating the activity of TCs in the western North Pacific (WNP). Numbers of evidences indicate that ENSO significantly influences TC genesis (Wu and Lau, 1992; Chan *et al.*, 2001; Wang and Chan, 2002), track (Wu *et al.*, 2004; Fudeyasu *et al.*, 2006; Zhang *et al.*, 2012), and intensity (Wang and Chan, 2002; Camargo *et al.*, 2007; Hong *et al.*, 2011; Li and Zhou, 2012) in the WNP. For example, strong El Niño (La Niña) enhances TC genesis in the southeastern (northwestern) quadrant of the WNP (Wang and Chan, 2002; Yonekura and Hall, 2014). More intense typhoons tend to occur during El Niño than La Niña because of the eastwards shift in TC genesis and a longer time spent over warmer water and within a moister environment (Wang and Chan, 2002; Zhang *et al.*, 2015). There are more recurring TCs during the El Niño than the La Niña phase (Wang and Chan, 2002; Hong *et al.*, 2011). The influence of ENSO on TC activity in the WNP results in the fact that landfalling TCs in East Asia are modulated by ENSO. The number of TCs landfalling in the landmasses rimming the WNP is significantly reduced during the late season (September–November) of El Niño years, with an exception for Japan and the Korean Peninsula (Wu *et al.*, 2004). More (less) TCs are likely to make landfall over China, Indochina, the Malay Peninsula, and the Philippines during the peak TC season (June–October) of La Niña (El Niño) years because of a westwards shift of TC genesis and of the subtropical high (Zhang *et al.*, 2012). Landfalling TCs in south China are associated with ENSO as well. A strong El Niño event reduces the number of landfalling TCs in south China whereas more TCs tend to make landfall in years associated with La Niña events (Liu and Chan, 2003; Saunders *et al.*, 2000; Wu *et al.*, 2004). Additionally, the chance of a TC striking the south China coast increases (decreases) significantly in May and June after a La Niña (El Niño) event (Liu and Chan, 2003).

The south China coast is one of the coastlines around the world that are most frequently affected by TCs (Chan *et al.*, 2004). Guangdong (GD) province, in the south of China, is the province with greatest occurrence of landfalling TCs in China. There are 3.9 landfalling TCs on average in GD every year, and up to a maximum of 7 in some years. Landfalling TCs frequently cause great losses to GD every year due to their rainfall. Therefore, it is necessary and beneficial to study the rainfall distribution of landfalling TCs in GD. Some studies (Yu *et al.*, 2015; Wen *et al.*, 2017) investigated the feature of rainfall distribution of landfalling TCs in GD. Yu *et al.* (2015) mainly compared the differences of TC rainfall asymmetry in different provinces over China. However, the characteristic of TC rainfall asymmetry in GD and its change in the process of making landfall were not clearly documented. In addition, there were only

22 landfalling TCs used for GD in their study. Wen *et al.* (2017) only focused the rainfall asymmetry on land after TC making landfall and its regional and seasonal differences in GD. This study focuses on TC rainfall asymmetry before, during, and after landfall and their influencing factors. This study is going to address four issues associated with the rainfall asymmetry of landfalling TCs in GD. What is the characteristic of rainfall asymmetry of landfalling TCs in GD? How does the TC rainfall asymmetry change in the process of making landfall? Is the rainfall asymmetry of landfalling TCs in GD related to storm motion or VWS? Is there difference in TC rainfall asymmetry during different ENSO phases? To answer these questions might help to improve TC rainfall forecast and reduce disaster loss in GD.

## 2 | DATA SET AND ANALYSIS METHODS

### 2.1 | Best track data, rainfall data, and ERA-Interim reanalysis data

Tropical cyclone best track data set from Shanghai Typhoon Institute, China Meteorological Administration (CMA) is used in this study. This data set provides 6-hourly information of TCs in the WNP (including South China Sea) since 1949. The information includes TC latitude, longitude, minimum centre pressure, and maximum sustained surface wind. In order to be consistent with the rainfall data, only the best track data from 1980 to 2015 are used in this study.

TRMM 3B42 precipitation data (Huffman *et al.*, 2007), version 7, is used to analyse the TC rainfall distribution. TRMM 3B42 data has 3-hourly temporal resolution and  $0.25 \times 0.25^\circ$  spatial resolution, covering the globe from  $50^\circ\text{S}$  to  $50^\circ\text{N}$ , available from 1998 to the present. Previous studies (Jiang *et al.*, 2008a; 2008b; Yu *et al.*, 2009; Chen *et al.*, 2013) have shown that TRMM 3B42 product could give quite reasonable rainfall patterns in landfalling TCs when compared with the gauge data or radar estimates. Some studies (Shen *et al.*, 2010; Zhao and Yatagai, 2014) indicated that TRMM 3B42 rainfall data performed reasonably well over south China.

Two different reanalysis precipitation data, the Modern-Era Retrospective analysis for Research and Applications, version 2 (MERRA2) and the European Centre for Medium-Range Weather Forecasts (ECMWF) interim reanalysis (ERA-Interim), are also utilized to validate the results based on TRMM satellite data. MERRA2 is the latest atmospheric reanalysis of the modern satellite era produced by NASA's Global Modeling and Assimilation Office (GMAO). MERRA2 features several major advances, including the use of observations-based precipitation data products to correct the precipitation and the allowance of the near-surface air temperature and humidity to respond to the improved precipitation forcing, which results in more self-consistent surface meteorological data (Reichle *et al.*, 2017). It has a native

resolution of  $0.5^\circ$  latitude  $\times$   $0.625^\circ$  longitude. Hourly time-average data since 1980 are analysed. The spatial resolution of ERA-Interim precipitation reanalysis data used is  $0.25 \times 0.25^\circ$  and the temporal resolution is 6-hourly.

ERA-Interim reanalysis data (Dee and Uppala, 2009) is used to calculate mean environmental VWS in this study. Only the meridional and zonal winds at 850 and 200-hPa levels are extracted. The horizontal resolution of the data is  $1.0 \times 1.0^\circ$  and the temporal resolution is 6-hourly.

## 2.2 | Methods

### 2.2.1 | Landfalling time and storm motion of TC

GD has a long coastline and is affected by TCs every year (Figure 1). There are 109 (54) TCs making landfall in GD during 1980–2015 (1998–2015). For some TCs, the landfalling time is not consistent with the recorded time in the best track data, since the data set is 6-hourly. If the actual landfalling time of a TC do not agree with the recorded time in best track data, the nearest recorded time is treated as landfalling time. For example, if a TC makes landfall at 0700 UTC (1000 UTC), 0600 UTC (1200 UTC) is regarded as landfall time. This study investigates the rainfall asymmetry of TCs before, during, and after making landfall. The period from 24 hr before landfall to 24 hr after landfall is treated as the process of making landfall in the study of Yu *et al.* (2015). However, a TC weakens quickly after landfall due to the friction of land surface and the cutting off of energy source. About 25% TCs used in this study has no record in best track data 18 hr after landfall. Therefore, the period from 24 hr before landfall to 12 hr after landfall is selected to study the TC rainfall asymmetry in this study.

Storm motion vector is calculated from TC centre position in best track data using a 6-hours centred differencing scheme. For a selected time, the storm motion vector is the average of the past and next 6-hours motion vectors based on adjacent two points. If there is no next (past) 6-hours

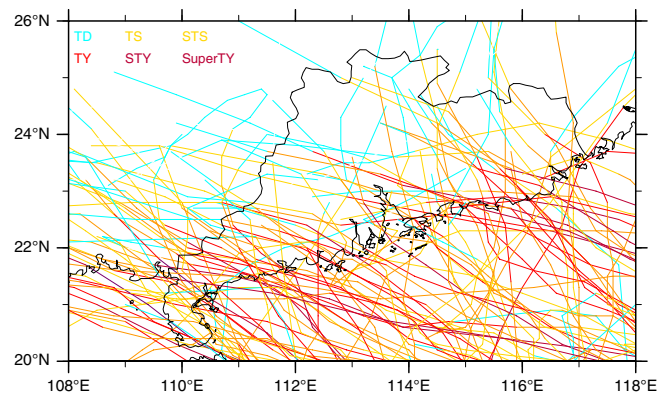


**FIGURE 1** Tracks of TCs making landfall in GD during 1980–2015. Storm intensity is indicated by different colours. Tropical depression (TD), tropical storm (TS), severe tropical storm (STS), typhoon (TY), severe typhoon (STY), and super typhoon (SuperTY) are indicated by cyan, yellow, orange, red, dark red, and purple, respectively [Colour figure can be viewed at [wileyonlinelibrary.com](http://wileyonlinelibrary.com)]

motion vector for the last (first) record of the track being at the selected time, the past (next) 6-hours motion vector is regards as the storm motion vector for the selected time.

### 2.2.2 | Rainfall interpolation

Following Lonfat *et al.* (2004) and Yu *et al.* (2015), the grid rainfall data is interpolated into storm-relative coordinate to show the rainfall distribution of TCs, since the centres of TCs are not the same. The coordinate is  $10 \text{ km} \times 1^\circ$  azimuth polar grid centred on the storm centre outwards to 500 km. After interpolation, the rainfall for each TC is in the same coordinate system, and it is convenient to make composite analysis for the rainfall distribution of TCs.

### 2.2.3 | Vertical wind shear

VWS is computed following the methodology of Hanley *et al.* (2001). The zonal and meridional winds at 850 and 200-hPa levels are first interpolated onto a  $100 \text{ km} \times 22.5^\circ$  azimuth polar grid centred on the storm centre outwards to 500 km, respectively. These winds are then averaged over a radius of 500 km from storm centre to remove symmetric vortex so that the winds provide a better measure of the environmental flow across the storm. The 200–850-hPa VWS is then calculated from these area-averaged winds over the inner 500 km of radius. This methodology was widely used to calculate VWS in other studies (Hanley *et al.*, 2001; Chan *et al.*, 2004; Qian *et al.*, 2016).

### 2.2.4 | Rainfall analysis

The rainfall distribution in a TC can be decomposed into axisymmetric and asymmetric components. We use Fourier transformation to decompose TC rainfall into wavenumber-0 component and a series of lower-wavenumber components of TC rainfall. The wavenumber-0 component, which is the azimuthal mean, represents the TC rainfall symmetry. The lower-wavenumber components depict the TC rainfall asymmetry. As will be found in section 3.1, wavenumber-1 rainfall asymmetry can depict the main feature of TC rainfall asymmetry. Thus wavenumber-1 Fourier coefficient is used to characterize the asymmetric rainfall distribution of TCs in this study. This method was widely used in studies (Lonfat *et al.*, 2004; Chen *et al.*, 2006; Yu *et al.*, 2015) on TC rainfall asymmetry.

As mentioned above, the TC rainfall in polar coordinate is in 10-km-wide annuli from TC centre to 500-km radius. In each annulus, the wavenumber-1 Fourier coefficients are computed using all rainfall in all azimuths:

$$a_1 = \sum_i [R_i \cos(\theta_i)] \text{ and } b_1 = \sum_i [R_i \sin(\theta_i)],$$

where  $R_i$  is the individual rainfall in each azimuth and  $\theta_i$  is the phase angle of the rainfall relative to azimuth reference. The azimuth reference can be either the spatial direction (e.g., the north), storm motion, or VWS. The wavenumber-1 rainfall asymmetric component can be represented by

$$M_1 = [a_1 \cos(\theta) + b_1 \sin(\theta)].$$

$M_1$  is the spatial distribution of wavenumber-1 rainfall component, which can display the TC rainfall asymmetry.

The azimuth reference is storm motion (VWS) when wavenumber-1 rainfall relative to storm motion (VWS) is calculated. However, the storm motion (VWS) of each TC is different. Thus the azimuth references are not the same. Same azimuth reference for each TC is needed to composite wavenumber-1 rainfall. Therefore, wavenumber-1 rainfall and storm motion (VWS) for each TC are rotated clockwise until the angle of storm motion (VWS) is at  $90^\circ$  in polar coordinate before composition. In addition, the wavenumber-1 rainfall relative to storm motion (VWS) means that the azimuth reference is storm motion (VWS) when Fourier transformation is performed.

## 3 | RESULTS

### 3.1 | TC rainfall asymmetry and main influencing factor

We first examine the rainfall distribution of landfalling TCs during 1998–2015 based on TRMM 3B42 rainfall data to provide an overview of TC rainfall asymmetry in GD. Figure 2a,d shows the average rainfall distributions of landfalling TCs in GD at different stages in the process of landfall. There are significant rainfall asymmetries in the TC rainfall distributions, and the asymmetric distributions are similar at different stages (Figure 2a,d). The rainfall distributions show that the southern side has more rainfall than the northern side, and the rainfall maximum is located in the south near the TC centre. This feature is more obvious from the distributions of wavenumber-1 rainfall in Figure 2e,h. The wavenumber-1 rainfall gives a better illustration for TC rainfall asymmetry. There are generally negative values in northern side and positive values in southern side for wavenumber-1 rainfall. The maximum of the wavenumber-1 rainfall is in the south near the TC centre as well. The distributions of average TC rainfall and wavenumber-1 rainfall indicate that the southern side of TC would have more rainfall for landfalling TCs in GD. What is more, the feature of rainfall maximum located in the south exists from 24 hr before landfall to 12 hr after landfall.

In addition to the phase (or position) of maximum rainfall, storm motion and VWS are relatively steady during the landfall process. In general, the storm motion is northwestwards, and the VWS is southwestwards (Figure 2). The rainfall maximum is located in the left or rear-left of storm motion (Figure 2). At the same time, the rainfall maximum lies in downshear left of VWS (Figure 2). From this point of view, both the storm motion and VWS could be the influencing factor of TC rainfall asymmetry in GD. In order to figure out the main influencing factor, we make a

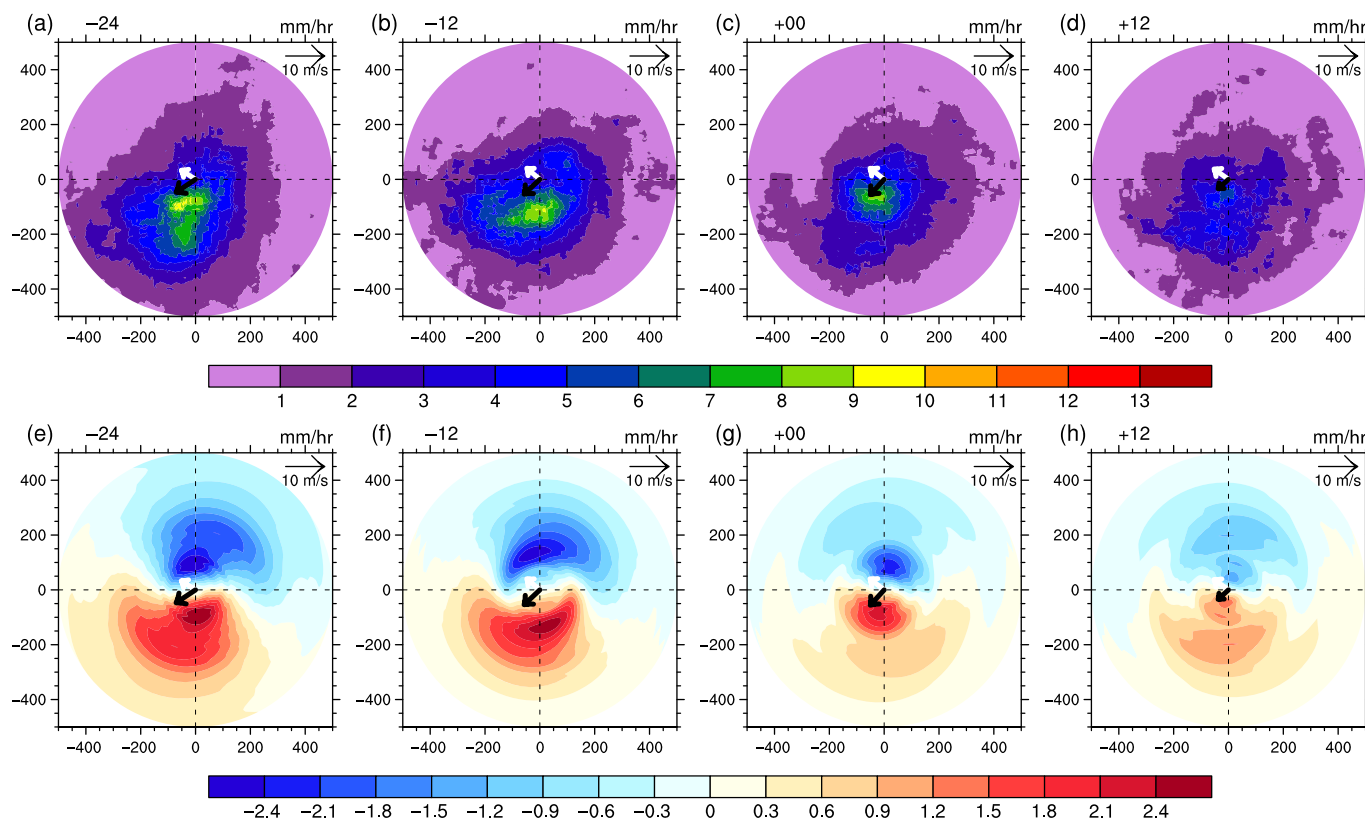


**FIGURE 2** Average TC rainfall (top row) and wavenumber-1 rainfall (bottom row) 24 hr prior to (left column), 12 hr prior to (second column), at the time of (third column), and 12 hr after landfall (right column) derived from TRMM 3B42 data. Black and white arrows represent VWS and storm motion, respectively [Colour figure can be viewed at [wileyonlinelibrary.com](http://wileyonlinelibrary.com)]

composite analysis of wavenumber-1 rainfall relative to storm motion and VWS, respectively.

The average storm motion of all landfalling TCs is northwestwards (Figure 2). Same as the average, most TCs have northwestwards storm motion as well. For example, 49 TCs out of 54 moved northwestwards 12 hr prior to landfall during 1998–2015 (Table 1). The northwest moving TCs are still the majority at other time (Table 1). Therefore, we divide landfalling TCs into two groups: northwest moving TCs, and non-northwest moving TCs. We composite the wavenumber-1 rainfall relative to storm motion for the two types of TCs. Since the distribution of wavenumber-1 rainfall of northwest moving TCs is quite similar with that for all TCs, we only show the average wavenumber-1 rainfall of all TCs and non-northwest moving TCs (Figure 3). It can be seen that there are positive values in the left side and negative values in the right side in the distribution of wavenumber-1 rainfall for all TCs. The rainfall maximum is located in the left or rear-left of storm motion. However, those for non-northwest moving TCs are totally different. There is no similar wavenumber-1 rainfall distribution for non-northwest moving TCs. More than that the wavenumber-1 rainfall distributions are diversified at different time and the locations of positive and negative values are disordered. The significant discrepancy of wavenumber-1 rainfall relative to storm motion between all TCs (or northwest moving TCs) and non-northwest moving TCs

indicates that the position of rainfall maximum relative to storm motion changes significantly as the direction of storm motion changes. Thus storm motion cannot well explain the TC rainfall asymmetry in GD. In addition, certain studies (Lonfat *et al.*, 2004; Chen *et al.*, 2010b) showed that the rainfall maximum is ahead of the storm centre on open sea or at the right of the track for a TC close to land when storm motion plays a leading role on rainfall asymmetry. However, the average maximum rainfall of all TCs is located in the left or rear-left of storm motion during the landfall process. Thus, storm motion could not be the main influencing factor of TC rainfall asymmetry in GD.

Figure 2 shows that the average VWS for all landfalling TCs is southwestwards. Table 1 also exhibits that most of the TCs, same as the average, have southwestwards VWS. Accordingly, TCs are classified into two groups based on the directions of VWS: TCs with southwestwards VWS, and TCs with non-southwestwards VWS. The wavenumber-1 rainfall relative to VWS is composited for all TCs, TCs with southwestwards VWS, and TCs with non-southwestwards VWS, respectively. The wavenumber-1 rainfall of TCs with southwestwards VWS is not displayed in Figure 4, since it is similar with that of all TCs. Figure 4a,d shows that there are positive values in downshear left and negative values in upshear right in the average wavenumber-1 rainfall of all TCs. The rainfall maximum occurs in downshear left of VWS. TCs with southwestwards VWS have almost the same

wavenumber-1 rainfall (not shown). Similarly, the wavenumber-1 rainfall of TCs with non-southwestwards VWS still have positive values in downshear left and negative values in upshear right. The rainfall maximum is steadily located in downshear left of VWS. These results indicate that the position of rainfall maximum relative to VWS changes little regardless of the variations of VWS. Therefore, the consistent rainfall asymmetry in different environmental VWS suggests that VWS is the main factor that determines the rainfall asymmetry of landfalling TCs in GD. The relative location of rainfall maximum is in downshear left of VWS. Since the average VWS shear is southwestwards (Figure 2), the position of downshear left is mainly in the south. This explains the preceding result that the spatial location of rainfall maximum is in the south of TC.

Some numerical studies (Frank and Ritchie, 1999; Rogers *et al.*, 2003; Ueno, 2007) suggested certain processes to explain the impact of VWS on TC rainfall asymmetry. These processes involve downshear tilt of TC vortex, a combination of downshear tilt and strength of TC vortex, the latent heat release due to water vapour saturation. However, they did not give a complete physical mechanism. Black *et al.* (2002) presented a physical mechanism to explain the VWS-induced rainfall asymmetry based upon observations. Differential advection of the axisymmetric vorticity by the shearing storm-relative flow induces a vertical motion dipole with ascent on the downshear side and descent on the upshear side (Frank and Ritchie, 2001). Convection form near the downshear side of the eyewall and move more slowly than the swirling wind. Convection cells grow as they move around the eye and reach maturity where the greatest rainfall occurred on the left side of VWS. When the hydrometeors advect farther around the eye and migrated outwards, the condensate fell out of them on the upshear right side. Therefore, the rainfall maximum is in downshear left of VWS.

The above analysis shows that wavenumber-1 rainfall clearly characterizes TC rainfall asymmetry in GD. However, It is unknown to what extent it depicts the actual TC rainfall asymmetry. Therefore, we compare the wavenumber-1 rainfall with total asymmetric rainfall, which is TC rainfall minus axisymmetric rainfall. The axisymmetric rainfall, that is the azimuthal mean, is represented by wavenumber-0 rainfall. Since VWS is the main influencing

factor of rainfall asymmetry, total asymmetric rainfall is derived relative to VWS as well. It can be seen from Figure 4i,l that total asymmetric rainfall also has positive values in downshear left and negative values in upshear right. Similar spatial patterns between wavenumber-1 rainfall (Figure 4a,d) and total asymmetric rainfall (Figure 4i,l) indicate that wavenumber-1 rainfall is able to depict the main feature of TC rainfall asymmetry in GD. Therefore, it is reasonable to use wavenumber-1 rainfall to analyse the rainfall asymmetry of TCs.

We extend our analysis to 1980 in order to examine the rainfall asymmetry with more TC samples using reanalysis precipitation data. There are 109 landfalling TCs in GD during 1980–2015. Same analysis method used above is applied to diagnosing the relationship between rainfall asymmetry and storm motion and VWS. Table 1 shows that northwestwards storm motion is the majority during 1980–2015. TCs are divided into northwest moving TCs and non-northwest moving TCs. We composite the wavenumber-1 rainfall relative to storm motion for the two types of TCs (figure not shown). Diverse wavenumber-1 rainfall distributions are found between the two groups of TCs, which agree with the result based on TRMM 3B42 data during 1998–2015. The result also supports that storm motion could not explain the rainfall asymmetry of landfalling TCs in GD.

Table 2 shows that most of VWSs are southwestwards during 1980–2015. Similarly, we classify landfalling TCs into two groups: TCs with southwestwards VWS and TCs with non-southwestwards VWS. Wavenumber-1 rainfall relative to VWS is composited for the two groups. The wavenumber-1 rainfall of TCs with southwestwards VWS is not displayed in Figure 5, since it is similar with that of all TCs. Figure 5a,d shows that average wavenumber-1 rainfall of all TCs (or TCs with southwestwards VWS) derived from MERRA2 data has positive values in downshear left and negative values in upshear right. The rainfall maximum is mainly located in downshear left of VWS. The distribution of wavenumber-1 rainfall of TCs with non-southwestwards VWS (Figure 5e,h) is similar with that of all TCs (or TCs with southwestwards VWS). The average wavenumber-1 rainfall of all TCs derived from ERA-Interim data also has positive values in downshear left and negative values in upshear right. Although it is a little different from that of all TCs, the wavenumber-1 rainfall of TCs with non-southwestwards VWS has positive values in downshear to downshear left and negative value in upshear to upshear right. Overall, these results are consistent with those derived from TRMM 3B42 rainfall during 1998–2015. The difference in the positions of positive values and negative values between MEERA2 and ERA-Interim data is probably related to the different temporal resolutions of two reanalysis data. Therefore, both satellite-based and reanalysis precipitation data support that VWS is the main factor that determines the

**TABLE 1** Number of landfalling TCs with northeastwards (NE), southeastwards (SE), southwestwards (SW), and northwestwards (NW) storm motion 24 hr prior to, 12 hr prior to, at the time of, 12 hr after landfall during 1998–2015 (1980–2015)

	NE	SE	SW	NW
–24 hr	6 (14)	0 (0)	2 (4)	46 (91)
–12 hr	4 (8)	0 (0)	1 (1)	49 (100)
0 hr	8 (12)	0 (0)	2 (2)	44 (95)
12 hr	8 (15)	0 (0)	6 (10)	33 (73)

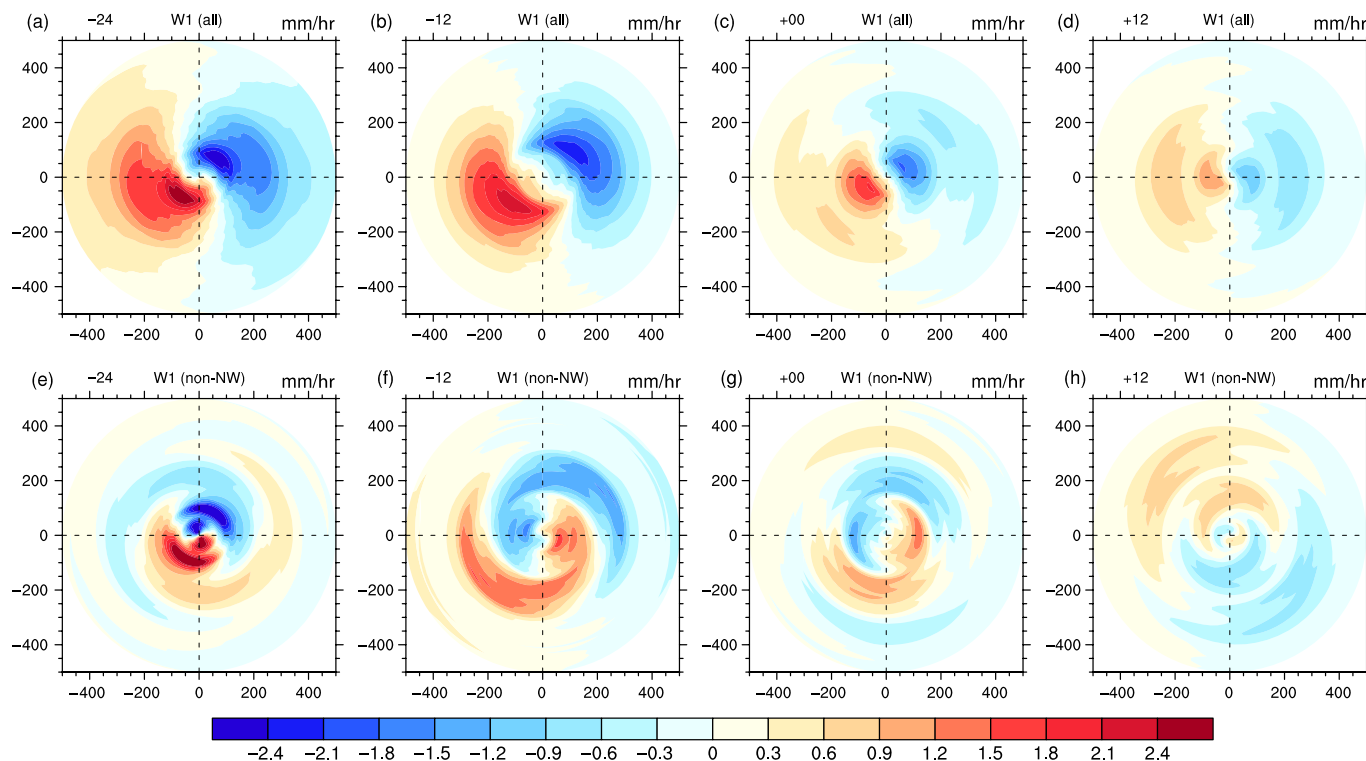


**FIGURE 3** Average wavenumber-1 rainfall relative to storm motion 24 hr prior to (left column), 12 hr prior to (second column), at the time of (third column), and 12 hr after landfall (right column) derived from TRMM 3B42 data. The top row is the average of all TCs, and the bottom row is the average of non-northwest moving TCs. The storm motion is pointed to the top in all panels [Colour figure can be viewed at [wileyonlinelibrary.com](http://wileyonlinelibrary.com)]

rainfall asymmetry of landfalling TCs in GD. The rainfall maximum is located in downshear left of VWS.

However, it should be noted that the wavenumber-1 rainfall in reanalysis data is weaker than that in satellite-based data. It is probably associated with a general defect in reanalysis system and atmospheric model. Models tend to underestimate heavy precipitation and overestimate light precipitation (Kimoto *et al.*, 2005; Dai, 2006; Sun *et al.*, 2006). Some evaluations also indicate that reanalysis products show similar systematic behaviours in overestimating small and medium precipitation amounts and underestimating high amounts (Pfeifroth *et al.*, 2012; Zhou and Wang, 2017). Still, the pattern of rainfall asymmetry and its relationship with VWS is reliable.

The analysis above reveals the average characteristics of TC rainfall asymmetry in GD using composite wavenumber-1 rainfall. We further discuss the significance of the composite results. We would like to know whether the composite rainfall asymmetry is able to represent the rainfall asymmetry of most TCs. Similar with Corbosiero and Molinari (2003), we calculate the wavenumber-1 rainfall at different octants and figure out the location (the octant) of the maximum wavenumber-1 rainfall for each TC. And then we count the number and proportion of TCs at each octant where the maximum wavenumber-1 rainfall is located during the process of landfall. Only the proportions, which are shown in Figure 6, are displayed since they are better to reflect the difference in quantity between different octants.

Figure 6a,c displays the proportions derived from TRMM data during 1998–2015. The bold numbers represent the octants in which the maximum wavenumber-1 rainfall is most frequently observed. These octants are referred to as the preferred octants where the TC rainfall maximum occurs. Figure 6a,c shows that the maximum wavenumber-1 rainfall, no matter within inner 100 km, the radii of 100–300 km, or 300–500 km, frequently occurs in downshear to downshear left of VWS, especially in downshear left. Up to 70.3, 82.5, and 65.4% of TCs have the maximum wavenumber-1 rainfall in downshear to downshear left within the radii of 0–100, 100–300, and 300–500 km, respectively. Of note is the very significant decrease in the proportions at the octants away from downshear. The proportions are consistent with the composite rainfall asymmetry based on satellite-based data. The proportions of TCs during 1980–2015 is calculated as well based on MERRA2 (Figure 6d,e) and ERA-Interim (Figure 6g,i) reanalysis data. The proportions derived from MERRA2 data are quite similar with those derived from TRMM data. Figure 6d,e shows that the octants in downshear to downshear left have the most frequent occurrence of maximum wavenumber-1 rainfall. The proportions there are 62.8, 71.2, and 61.2% within the radii of 0–100, 100–300, and 300–500 km, respectively. The proportions are consistent with the composite rainfall asymmetry based on MERRA2 data as well. The proportions derived from ERA-Interim data have slight difference with those based MERRA2 and TRMM data. The proportions are

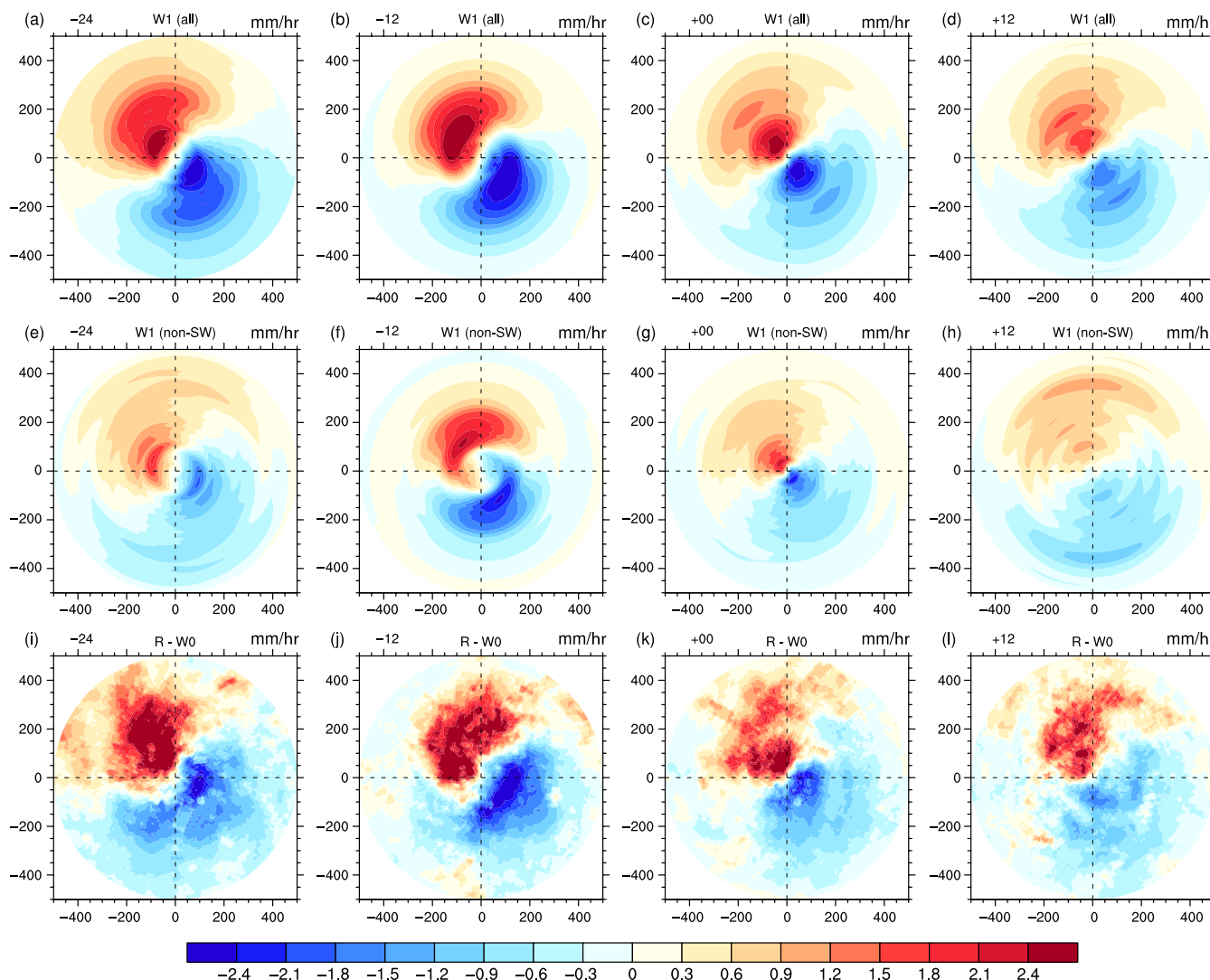


**FIGURE 4** Average wavenumber-1 rainfall (top two rows) relative to VWS and TC rainfall minus axisymmetric (wavenumber-0) rainfall (bottom row) 24 hr prior to (left column), 12 hr prior to (second column), at the time of (third column), and 12 hr after landfall (right column) derived from TRMM 3B42 data. The top row is the average of all TCs, and second row is the average of TCs with non-southwestwards VWS. The VWS is pointed to the top in all panels [Colour figure can be viewed at [wileyonlinelibrary.com](http://wileyonlinelibrary.com)]

in downshear left to left within the radii of 100–300 and 300–500 km. These are associated with the temporal resolution of ERA-Interim data as mentioned earlier. Still, the proportions are consistent with the composite rainfall asymmetry based on ERA-Interim data. The total proportions are 56.8, 69.7, and 63.6% in the preferred octants in which maximum wavenumber-1 rainfall occurs. These results based on satellite-based data and reanalysis data indicate that the composite rainfall asymmetry is able to reflect the rainfall asymmetry of most TCs.

**TABLE 2** Same as Table 1, but for VWS

	NE	SE	SW	NW
-24 hr	2 (7)	3 (7)	39 (75)	10 (20)
-12 hr	5 (14)	5 (9)	39 (72)	5 (14)
0 hr	4 (14)	7 (12)	35 (70)	8 (13)
12 hr	8 (18)	5 (14)	28 (54)	6 (12)

### 3.2 | Change in TC rainfall asymmetry in the process of making landfall

The overall TC rainfall asymmetry in GD has been revealed in front. Change in TC rainfall asymmetry in the process of making landfall is still our concern. Only satellite-based precipitation data is used to analyse change in rainfall asymmetry, since reanalysis precipitation data has a defect in intensity. Figure 7 displays the quadrant average rainfall at different radii from centre to outwards. The quadrants are relative to VWS, since VWS is the main influencing factor of TC rainfall asymmetry. Figure 7a shows that the quadrant average rainfall within inner 500 km decreases in the process of making landfall in all quadrants, including downshear left, downshear right, upshear left, and upshear right. The axisymmetric (wavenumber-0) and asymmetric (wavenumber-1) rainfall in downshear left also has a significant decrease. These results are consistent with the spatial distributions of TC rainfall in Figure 2 and wavenumber-1 rainfall

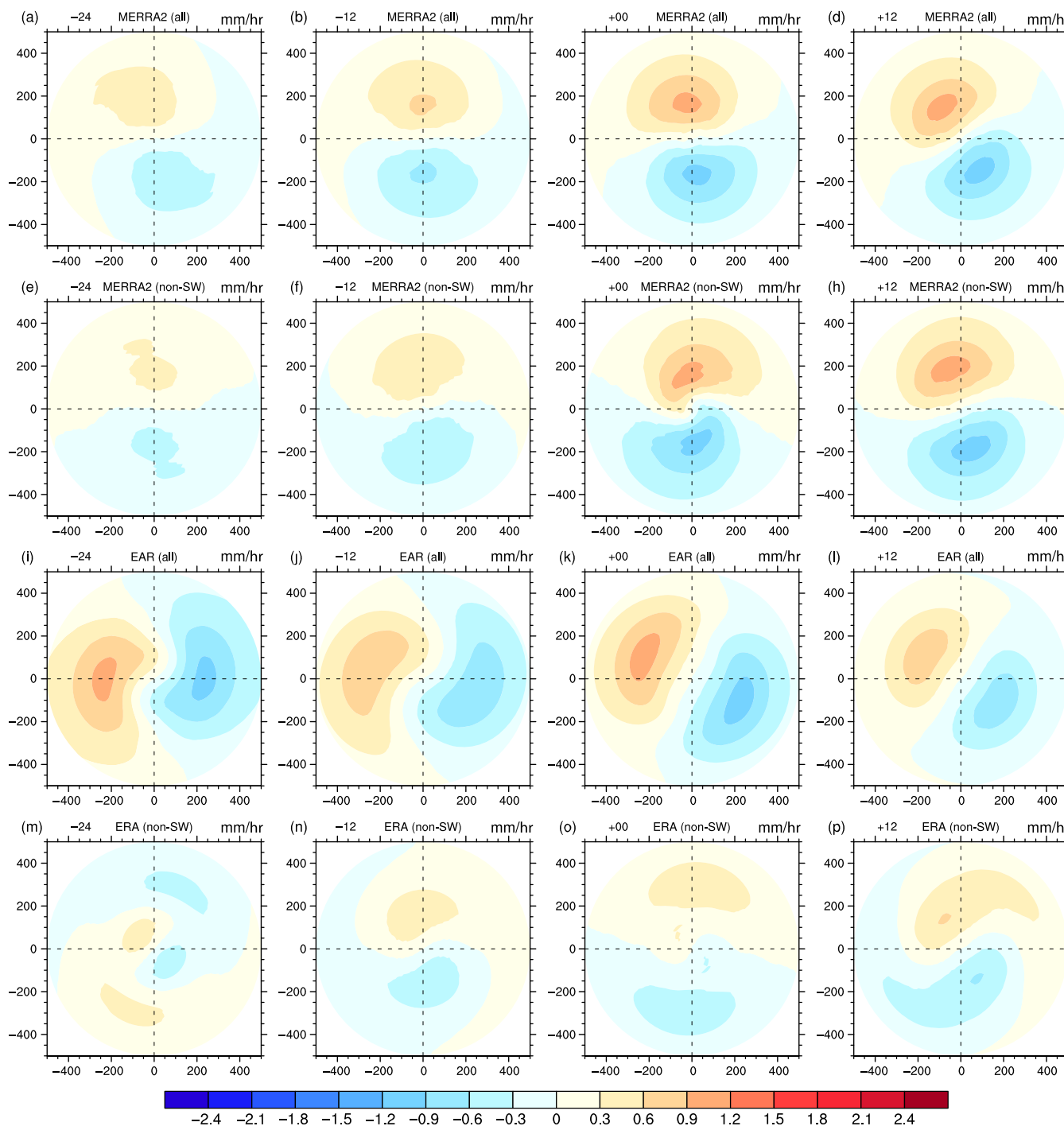


**FIGURE 5** Average wavenumber-1 rainfall relative to VWS 24 hr prior to (left column), 12 hr prior to (second column), at the time of (third column), and 12 hr after landfall (right column) derived from MERRA2 (top two rows) and ERA-Interim (bottom two rows) reanalysis data. The top row and the third row are the average of all TCs, and the second row and the bottom row are the average of TCs with non-southwestwards VWS. The VWS is pointed to the top in all panels [Colour figure can be viewed at [wileyonlinelibrary.com](http://wileyonlinelibrary.com)]

in Figure 4, where the rainfall shows an obvious decrease in the process of making landfall. What is more, the decrease in rainfall is also seen at different radii from centre to outwards (Figure 7b,d). There are generally decrease trends within the radii of 0–100 km (Figure 7b), 100–300 km (Figure 7c), and 300–500 km (Figure 7d), especially after making landfall (0–12 hr). In general, TC rainfall decreases from centre to outwards in the process of making landfall. That is because

friction of land and the cutting off of energy source cause TC to weaken.

Another distinct feature is that the downshear left quadrant almost has the largest rainfall during TC landfall process (Figure 7). The rainfall in downshear left is significant larger than that in other quadrants. For example, the average rainfall in downshear left (~4.1 mm/hr) is nearly twice of that in downshear right (~2.3 mm/hr) or upshear left (~2.2 mm/hr) at 24 hr prior to landfall. This feature can also be seen from

the distributions of TC rainfall at different stages (Figure 2a, d), where the rainfall always leans to downshear left of VWS. In addition, the positive values in wavenumber-1 rainfall relative to VWS are invariably located in downshear left of VWS as well (Figure 4a,d). These results indicate that the phase of TC rainfall asymmetry in GD hardly changes in the process of making landfall.

We further analyse the change in the amplitude of TC rainfall asymmetry. Following Chen *et al.* (2006), the amplitude of TC rainfall asymmetry is defined as the ratio between wavenumber-1 rainfall (asymmetric component) and wavenumber-0 rainfall (axisymmetric component) in downshear left. Figure 8 displays the amplitude of rainfall asymmetry in the process of TC making landfall. It can be seen from Figure 8a,d that the largest amplitude of rainfall asymmetry is within the radius of 100–300 km. The amplitude is up to 60% (Figure 8e), implying that the wavenumber-1 rainfall (asymmetric rainfall) reaches up to 60% of wavenumber-0 rainfall (axisymmetric rainfall). The inner area (0–100 km) has smaller rainfall asymmetry amplitude, which is about 40% (Figure 8a,e). The rainfall asymmetry amplitude in outwards area (300–500 km) has small variation in the landfall process at the range of 20–50%. The overall rainfall asymmetry amplitude within inner 500 km is about 50%, suggesting that the asymmetric rainfall is half of the axisymmetric rainfall. Although there are some differences, the variations in the amplitude of rainfall asymmetry are small in the process of making landfall based on the spatial distributions in Figure 8a,d. The quadrant average also indicates that the amplitude has no significant change from 24 hr prior to landfall to 12 hr after landfall. The amplitudes of rainfall asymmetry also hardly change at different radii from centre to outwards (Figure 8e). These results make sense since the VWS, the main factor influencing rainfall asymmetry, is relatively stable in the process of making landfall (Figure 2).

In general, although TC rainfall decreases, the phase and amplitude of TC rainfall asymmetry have no significant change in the process of making landfall.

### 3.3 | TC rainfall asymmetry in El Niño and La Niña years

ENSO strongly impacts the climate and weather in WNP and East Asia (Lau and Nath, 2000; Wang *et al.*, 2003; Wu *et al.*, 2003; Karori *et al.*, 2013; Hu *et al.*, 2014). The large-scale circulation is quite diverse during different ENSO phases (Wang *et al.*, 2000; Wu *et al.*, 2010; Karori *et al.*, 2013). Thus we further investigate the TC rainfall asymmetry in GD during El Niño and La Niña years. The entire 36-year period from 1980 to 2015 is subdivided into El Niño years, La Niña years, and neutral years according to Oceanic Niño Index (ONI) of TC season (July–September). The ONI is 3-month running mean of ERSST.v5 SST anomalies in the Niño3.4 region (5°N–5°S, 120°–170°W). It is El Niño

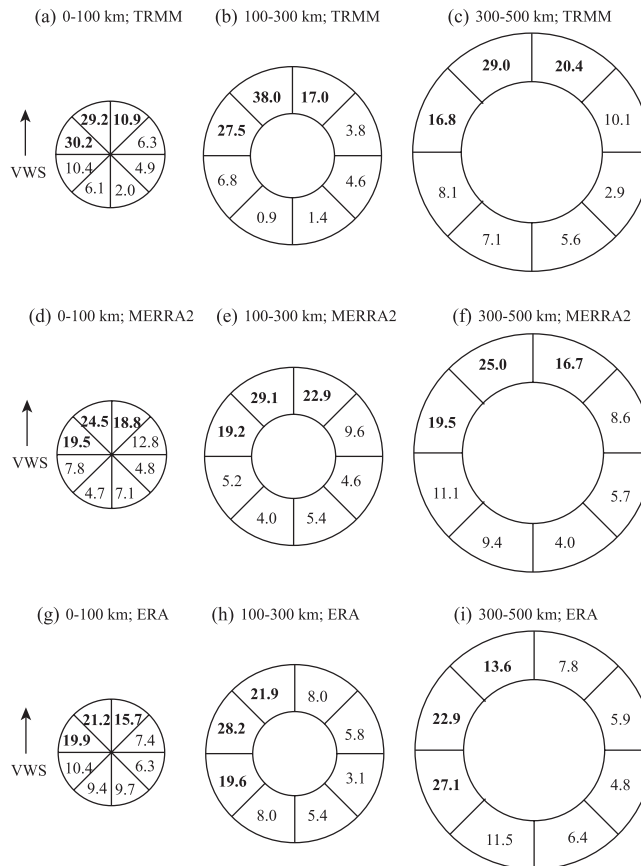


**FIGURE 6** Proportion (unit: %) of TCs at each octant where the maximum wavenumber-1 rainfall is located during the process of landfall within the radii of 0–100 km (left column), 100–300 km (centre column), and 300–500 km (right column), derived from TRMM 3B42 data (top row), MERRA2 data (centre row), and ERA-Interim data (bottom row), respectively. The three largest proportions are shown in bold font. The VWS is pointed to the top in all panels

(La Niña) year when ONI is equal or greater (less) than 0.5 (–0.5). It is neutral year when ONI range from –0.4 to 0.4. The classification is given in Table 3. There are 4 (9) El Niño years, 6 (9) La Niña years, 8 (18) neutral years during 1998–2015 (1980–2015).

Table 4 shows the proportion of VWS in different directions during 1998–2015 and 1980–2015. Southwestwards VWS dominants no matter whether it is El Niño year or La Niña year. There are 60–70% southwestwards VWS. Although El Niño years have a slight more northeastwards VWS and less southeastwards VWS than La Niña years, they only account for a small proportion. In general, there is no significant difference in VWS in different ENSO phases.

Figure 9 displays spatial distributions of average wavenumber-1 rainfall during El Niño, La Niña, and neutral years derived from satellite-based data and reanalysis data. TRMM 3B42 data shows that distributions of wavenumber-1 rainfall are quite similar between El Niño, La Niña, and neutral years (Figure 9a,c). There are no differences in the patterns of wavenumber-1 rainfall. They are characterized

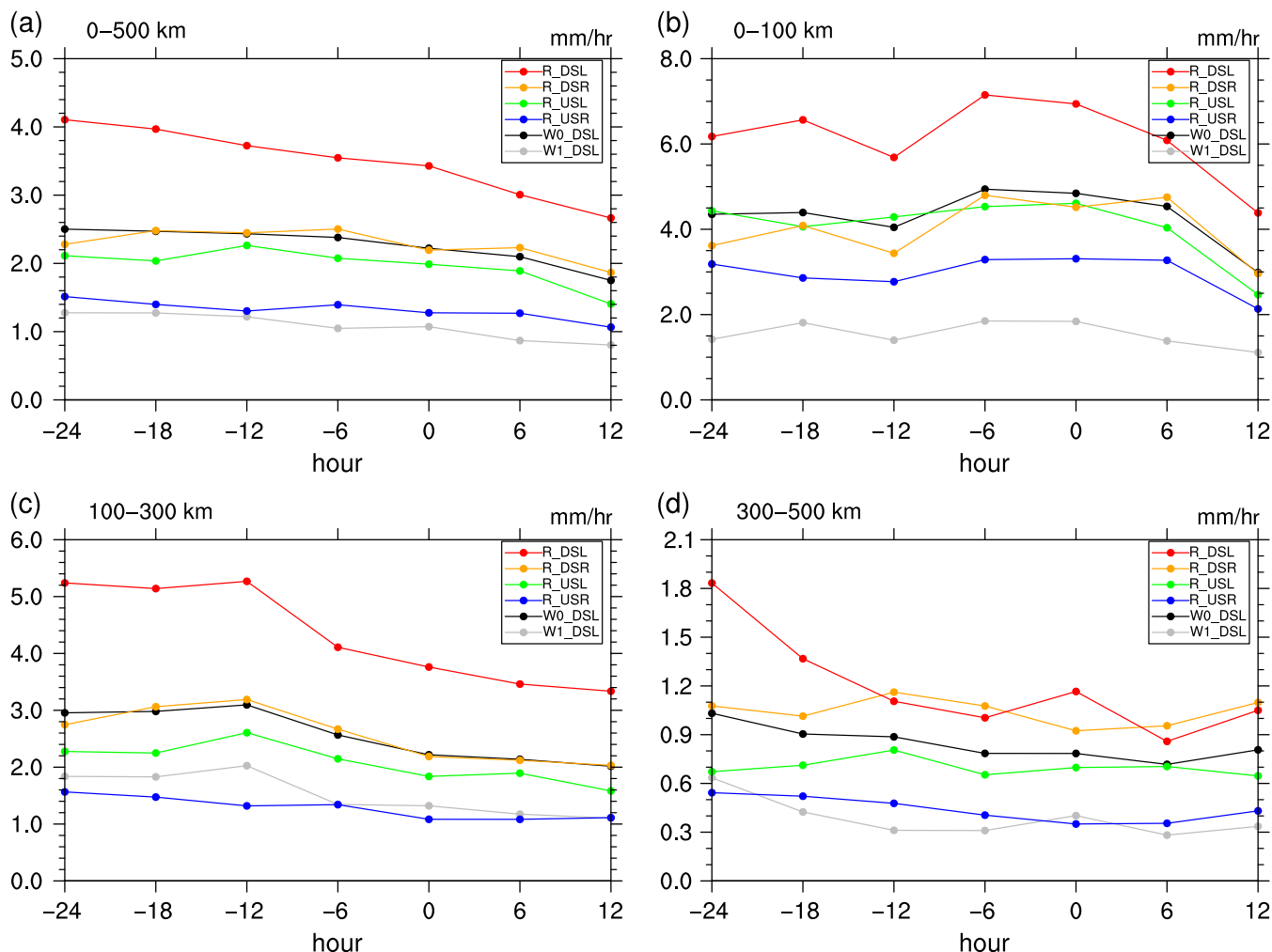


**FIGURE 7** Quadrant average rainfall, wavenumber-0, and wavenumber-1 rainfall derived from TRMM 3B42 data from 24 hr prior to landfall to 12 hr after landfall within the radii of 0–500 km (a), 0–100 km (b), 100–300 km (c), 300–500 km (d). Red, orange, green, blue, black, and grey lines represent rainfall in downshear left (R\_DSL), downshear right (R\_DSR), upshear left (R\_USL), upshear right (R\_USR), wavenumber-0 rainfall (W0\_DSL), and wavenumber-1 rainfall (W1\_DSL), respectively [Colour figure can be viewed at [wileyonlinelibrary.com](http://wileyonlinelibrary.com)]

by positive values in the south and negative values in the north. Reanalysis data also indicates that there are remarkable resemblance in the features of wavenumber-1 rainfall between El Niño, La Niña, and neutral years. MERRA2 data shows that wavenumber-1 rainfall has positive values in the south and negative values in the north in El Niño, La Niña, and neutral years (Figure 9d, f). This feature is analogous to that derived from TRMM data. The wavenumber-1 rainfall derived from ERA-Interim data also has similar features in different ENSO phases (Figure 9g, i). The positive values are in the southeast quadrant and negative values are in the northwest quadrant. The phases of positive values and negative values are a little different with those in MERRA2 data. It is associated with the temporal resolution of ERA-Interim precipitation data and the movement of TCs. ERA-Interim precipitation is the cumulative rainfall over the past 6 hr. In addition, most of TCs have a northwards moving track. Therefore the rainfall maximum is in southeastern quadrant. Both satellite-based data and

reanalysis data indicate that there is no obvious difference in TC rainfall asymmetry between different ENSO phases.

The relationship between rainfall asymmetry and VWS in El Niño, La Niña, and neutral years is examined as well. Figure 10 displays the average wavenumber-1 rainfall relative to VWS in El Niño, La Niña, and neutral years derived from satellite-based data and reanalysis data. TRMM data shows that the wavenumber-1 rainfall has the same features in El Niño, La Niña, and neutral years (Figure 10a, c). It is characterized by positive values in downshear left and negative values in upshear right. The rainfall maximum is in downshear left of VWS. Thus satellite-based data indicates that there is no difference in TC rainfall asymmetry between El Niño, La Niña, and neutral years. Reanalysis data also shows similar feature. Both MERRA2 (Figure 10d, f) and ERA-Interim (Figure 10g, i) reanalysis precipitation data show that there is no significant difference in wavenumber-1 rainfall in different ENSO phases. The patterns of wavenumber-1 rainfall are quite similar between El Niño, La

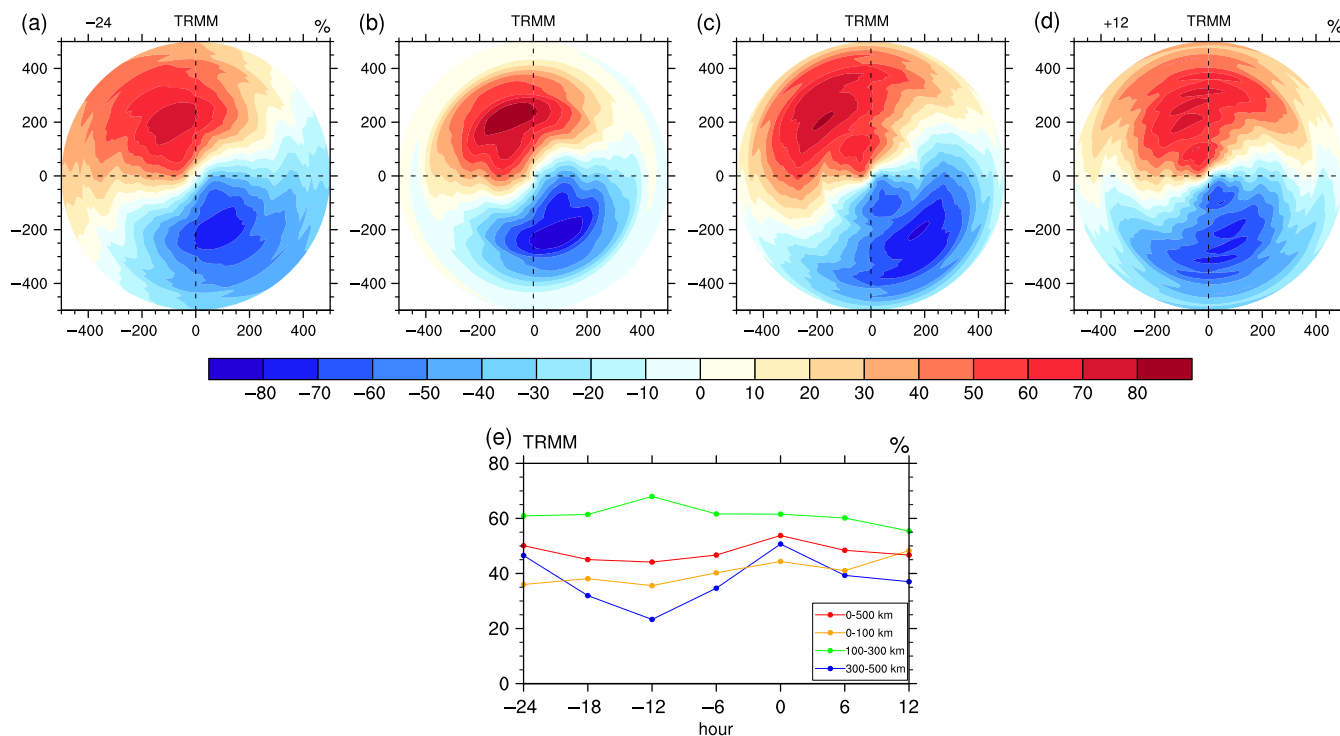


**FIGURE 8** Average amplitude ( $W1/W0$ ) of rainfall asymmetry 24 hr prior to (a), 12 hr prior to (b), at the time of (c), and 12 hr after landfall (d) and quadrant average amplitude (e) of rainfall asymmetry in downshear left from 24 hr prior to landfall to 12 hr after landfall within the radii of 0–500 km (red), 0–100 km (orange), 100–300 km (green), and 300–500 km (blue) [Colour figure can be viewed at [wileyonlinelibrary.com](http://wileyonlinelibrary.com)]

**TABLE 3** Years classified according to ONI of TC season (JAS)

El Niño	La Niña	Neutral
1982	1985	1980
1986	1988	1981
1987	1995	1983
1991	1998	1984
1997	1999	1989
2002	2000	1990
2004	2007	1992
2009	2010	1993
2015	2011	1994
		1996
		2001
		2003
		2005
		2006
		2008
		2012
		2013
		2014

**TABLE 4** Percentage of VWS in different directions during 1998–2015 (1980–2015)

	NE	SE	SW	NW
El Niño	17.5 (17.5)	5.0 (8.4)	67.5 (55.9)	10.0 (18.2)
La Niña	7.5 (10.9)	10.3(11.6)	63.6 (61.7)	18.6 (15.8)
Neutral	6.7 (11.6)	10.0 (7.8)	72.2 (70.6)	11.1 (10.0)

Niña, neutral years. Positive values are generally in downshear left and negative values are in upshear right. The difference in the positions of positive values and negative values between MEERA2 and ERA-Interim data is related to the difference in temporal resolution of data. Thus, VWS is still the main influencing factor of rainfall asymmetry of landfalling TCs in GD no matter in El Niño years or La Niña years.

#### 4 | SUMMARY AND DISCUSSION

In this study, we investigate the rainfall asymmetry of TCs in the process of making landfall in GD based on best track data and satellite-based and reanalysis precipitation data. TC rainfall is decomposed into different wavenumber components through Fourier transformation. Same as previous studies (Lonfat *et al.*, 2004; Chen *et al.*, 2006; Yu *et al.*, 2015), wavenumber-1 rainfall is used to analyse the TC rainfall asymmetry, since it has a similar distribution with TC rainfall minus axisymmetric rainfall (wavenumber-0 rainfall).

We first composite the rainfall distribution of landfalling TCs in GD and their storm motion and VWS. It is found that there is more rainfall in the southern side than the northern side of TC and the rainfall maximum is in the south near the centre. In order to figure out the relationship between rainfall asymmetry and storm motion and VWS, TCs are classified into different group based on storm motion and VWS,

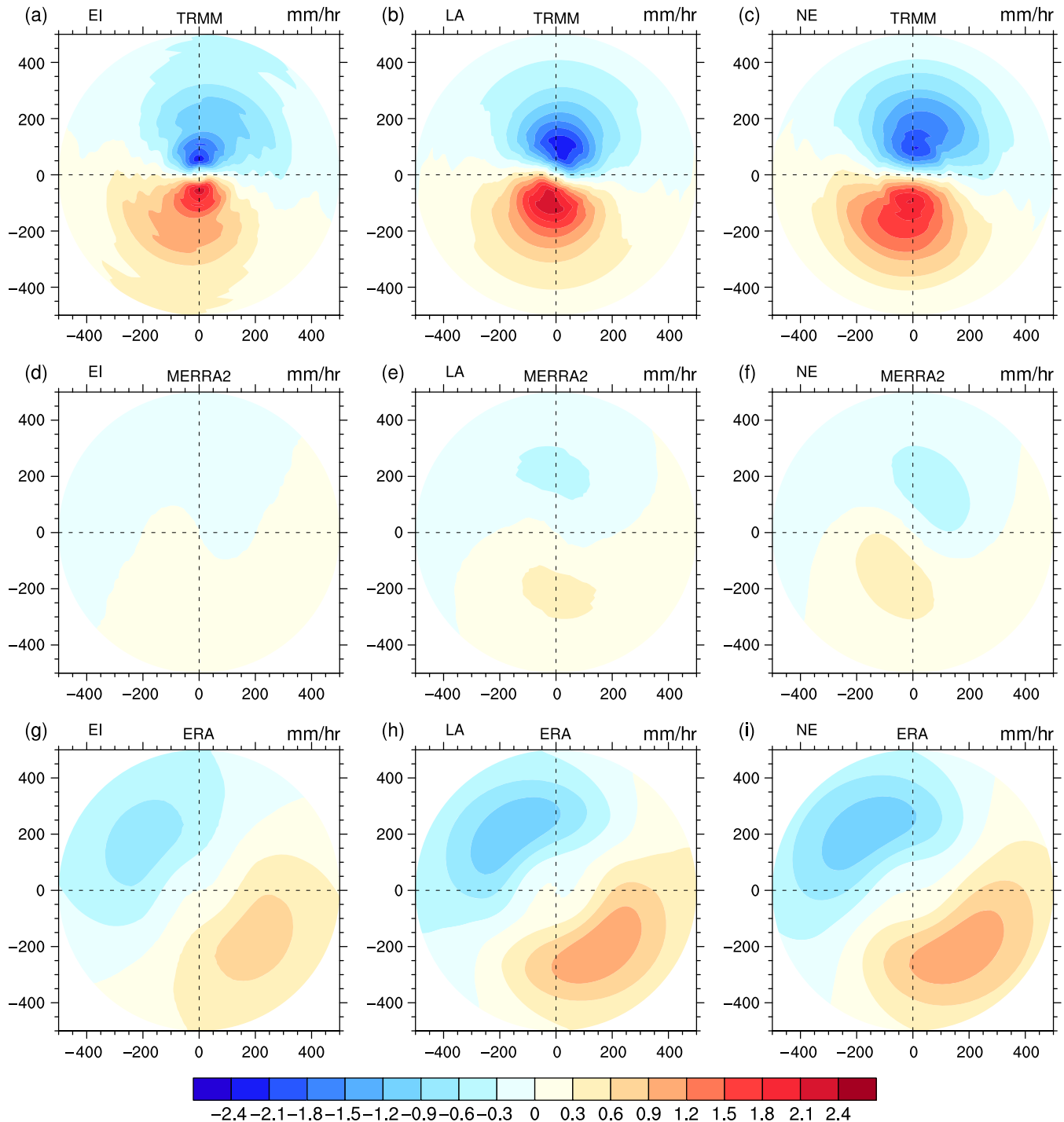


**FIGURE 9** Average wavenumber-1 rainfall during El Niño (left column), La Niña (centre column), and neutral (right column) years derived from TRMM 3B42 data (top row), MERRA2 (centre row), and ERA-Interim (bottom row) reanalysis data [Colour figure can be viewed at [wileyonlinelibrary.com](http://wileyonlinelibrary.com)]

respectively. The wavenumber-1 rainfall relative to storm motion is quite different between northwest moving TCs and non-northwest moving TCs. The position of rainfall maximum relative to storm motion changes significantly as the storm motion changes. This indicates that storm motion cannot explain the rainfall asymmetry of TCs in GD. On the contrary, TCs with southwestwards VWS and TCs with non-southwestwards VWS have similar distributions of wavenumber-1 rainfall relative to VWS. Wavenumber-1 rainfall relative to VWS changes little as VWS changes. The

consistent rainfall asymmetry in different VWS implies that VWS is the main influencing factor of TC rainfall asymmetry in GD. The rainfall maximum is located in downshear left of VWS.

In addition, we analyse the change in rainfall asymmetry of TCs in the process of making land in GD. The rainfall decreases during the landfall process, especially after making landfall. However, the location of rainfall maximum is consistently in downshear left from 24 hr prior to landfall to 12 hr after landfall. The amplitude of rainfall asymmetry,

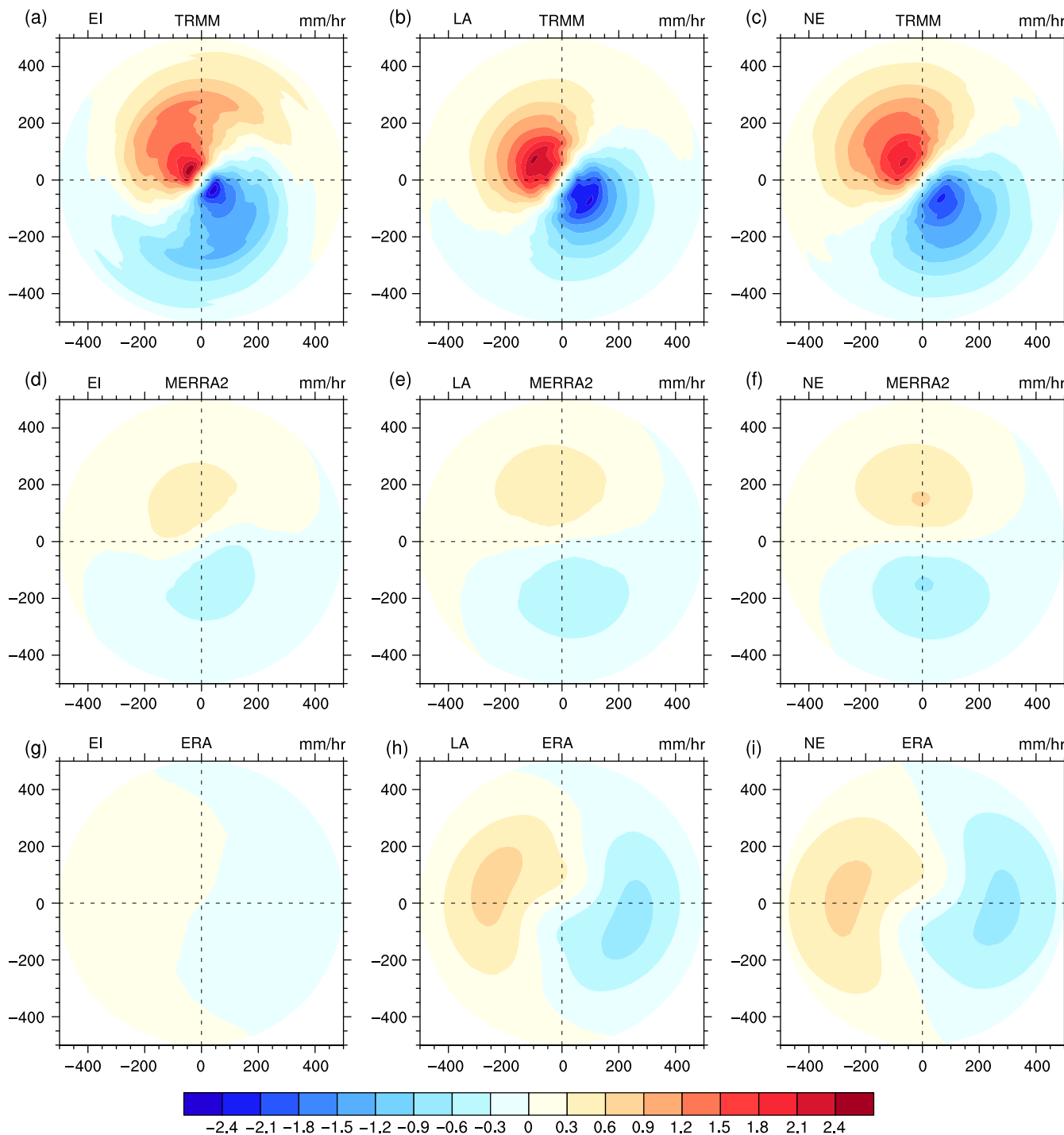


**FIGURE 10** Average wavenumber-1 rainfall relative to VWS during El Niño (left column), La Niña (centre column), and neutral (right column) years derived from TRMM 3B42 data (top row), MERRA2 (centre row), and ERA-Interim (bottom row) reanalysis data. The VWS is pointed to the top in all panels [Colour figure can be viewed at [wileyonlinelibrary.com](http://wileyonlinelibrary.com)]

which is defined as the ratio between wavenumber-1 (asymmetric) rainfall and wavenumber-0 (axisymmetric) rainfall, has no significant change in the process of landfall as well. The area within the radius of 100–300 km has the largest amplitude of rainfall asymmetry, which is about 60%. The average amplitude is about 50% within inner 500 km, suggesting that the asymmetric rainfall is about half of the axisymmetric rainfall.

We finally analyse the difference in rainfall asymmetry of landfalling TCs in different ENSO phases. Both satellite-based data and reanalysis data indicate that there is no obvious difference in TC rainfall asymmetry between El Niño, La Niña, and neutral years. VWS is the main influencing factor of rainfall asymmetry of landfalling TCs in GD whether in El Niño, La Niña, or neutral years. The rainfall maximum consistently lies in downshear left of VWS.

The rainfall asymmetry and main influencing factor of GD is consistent with those over south China reported by Xu *et al.* (2014). However, the two areas are not the same, although two areas have some overlaps. Xu *et al.* (2014) reported the TC rainfall asymmetry and its association with VWS based on the composited total TC rainfall and its relative location to VWS and storm motion. In addition to total TC rainfall, wavenumber-1 rainfall is used to display the rainfall asymmetry in this study. The wavenumber-1 rainfall gives a better illustration for TC rainfall asymmetry than total TC rainfall as used by Xu *et al.* (2014). What is more, we divide TCs in different groups based on VWS to examine the relationship between rainfall asymmetry and VWS. We find the relative location of maximum rainfall to VWS is the same in different VWSs. The result in this study gives a more robust relationship between rainfall asymmetry and VWS than that in the study of Xu *et al.* (2014). Last but not the least, this study reveals the change in the amplitude of TC rainfall asymmetry in the process of making landfall, which is not involved in the study of Xu *et al.* (2014). Although Yu *et al.* (2015) analysed the TC rainfall asymmetry in GD, the characteristic of TC rainfall asymmetry in GD was not clearly documented. They mainly compared the rainfall asymmetry in different regions of China and found a cyclonic rotation of rainfall maximum from south China to east China. In addition, there are only 22 landfalling TCs over GD and 15 TCs 24 hr after landfall in the study of Yu *et al.* (2015), which is far less than the 109 TCs used in this study. Furthermore, the method that we use to examine the relationship between rainfall asymmetry and VWS is more elaborate. More TCs used and more elaborate analysis make the results of this study more robust.

GD is the province that has the most landfalling TCs in China. This study reveals the rainfall asymmetry, its main influencing factor, its change in the process of landfall, and its difference between different ENSO phases in GD. Results of this study can increase the scientific understanding of TC rainfall asymmetry in GD. More importantly, they are useful for making prediction of rainfall distribution, especially the heavy rainfall area of landfalling TCs.

#### ACKNOWLEDGEMENTS

This work was supported by National Basic Research Program of China (2015CB452802), Natural Science Foundation of Guangdong Province (2016A030310009), National Natural Science Foundation of China (41675021, 41675019, 41475061, 41425019, and 41475102), Guangzhou Science and Technology Plan Project (201510010218), and Scientific and Technological Research Project of Guangdong Meteorological Service (GRMC2018M05).

#### ORCID

Guanhuan Wen  <https://orcid.org/0000-0003-3139-579X>

#### REFERENCES

- Bjerknes, J. (1969) Atmospheric teleconnections from the equatorial Pacific. *Monthly Weather Review*, 97(3), 163–172. [https://doi.org/10.1175/1520-0493\(1969\)097<0163:ATFTEP>2.3.CO;2](https://doi.org/10.1175/1520-0493(1969)097<0163:ATFTEP>2.3.CO;2).
- Black, M.L., Gamache, J.F., Marks, F.D., Samsury, C.E. and Willoughby, H.E. (2002) Eastern Pacific Hurricanes Jimena of 1991 and Olivia of 1994: the effect of vertical shear on structure and intensity. *Monthly Weather Review*, 130(9), 2291–2312. [https://doi.org/10.1175/1520-0493\(2002\)130<2291:EPHJOA>2.0.CO;2](https://doi.org/10.1175/1520-0493(2002)130<2291:EPHJOA>2.0.CO;2).
- Burpee, R.W. and Black, M.L. (1989) Temporal and spatial variations of rainfall near the centers of two tropical cyclones. *Monthly Weather Review*, 117(10), 2204–2218. [https://doi.org/10.1175/1520-0493\(1989\)117<2204:TASVOR>2.0.CO;2](https://doi.org/10.1175/1520-0493(1989)117<2204:TASVOR>2.0.CO;2).
- Camargo, S.J., Robertson, A.W., Gaffney, S.J., Smyth, P. and Ghil, M. (2007) Cluster analysis of typhoon tracks. Part II: large-scale circulation and ENSO. *Journal of Climate*, 20(14), 3654–3676. <https://doi.org/10.1175/JCLI4203.1>.
- Chan, J.C.L. (2008) A simple seasonal forecast update of tropical cyclone activity. *Weather and Forecasting*, 23(5), 1016–1021. <https://doi.org/10.1175/2008WAF2007061.1>.
- Chan, J.C.L., Shi, J.-E. and Liu, K.S. (2001) Improvements in the seasonal forecasting of tropical cyclone activity over the western North Pacific. *Weather and Forecasting*, 16(4), 491–498. [https://doi.org/10.1175/1520-0434\(2001\)016<0491:IITTSFO>2.0.CO;2](https://doi.org/10.1175/1520-0434(2001)016<0491:IITTSFO>2.0.CO;2).
- Chan, J.C.L., Liu, K.S., Ching, S.E. and Lai, E.S.T. (2004) Asymmetric distribution of convection associated with tropical cyclones making landfall along the south China coast. *Monthly Weather Review*, 132(10), 2410–2420. [https://doi.org/10.1175/1520-0493\(2004\)132<2410:ADOCAW>2.0.CO;2](https://doi.org/10.1175/1520-0493(2004)132<2410:ADOCAW>2.0.CO;2).
- Chang, C.-P., Lei, Y., Sui, C.-H., Lin, X. and Ren, F. (2012) Tropical cyclone and extreme rainfall trends in East Asian summer monsoon since mid-20th century. *Geophysical Research Letters*, 39(18), L18702. <https://doi.org/10.1029/2012GL052945>.
- Chen, Q.-Z. and Fang, J. (2012) Effects of vertical wind shear on intensity and structure of tropical cyclone. *Journal of Tropical Meteorology*, 18(2), 172–186. <https://doi.org/10.3969/j.issn.1006-8775.2012.02.007>.
- Chen, S.S., Knaff, J.A. and Marks, F.D. (2006) Effects of vertical wind shear and storm motion on tropical cyclone rainfall asymmetries deduced from TRMM. *Monthly Weather Review*, 134(11), 3190–3208. <https://doi.org/10.1175/MWR3245.1>.
- Chen, L., Li, Y. and Cheng, Z. (2010a) An overview of research and forecasting on rainfall associated with landfalling tropical cyclones. *Advances in Atmospheric Sciences*, 27(5), 967–976. <https://doi.org/10.1007/s00376-010-8171-y>.
- Chen, L., Xu, H., Yu, H., Qi, L., Luo, X. and Xu, X. (2010b) Temporal and spatial variations in precipitation of typhoon Saomai (0608) before and after its landfall. *Chinese Journal of Atmospheric Sciences*, 34(1), 105–119 (in Chinese).
- Chen, Y., Ebert, E.E., Walsh, K.J.E. and Davidson, N.E. (2013) Evaluation of TRMM 3B42 precipitation estimates of tropical cyclone rainfall using PACRAIN data. *Journal of Geophysical Research: Atmospheres*, 118(5), 2184–2196. <https://doi.org/10.1002/jgrd.50250>.
- Corbosiero, K.L. and Molinari, J. (2002) The effects of vertical wind shear on the distribution of convection in tropical cyclones. *Monthly Weather Review*, 130(8), 2110–2123. [https://doi.org/10.1175/1520-0493\(2002\)130<2110:TEOVWS>2.0.CO;2](https://doi.org/10.1175/1520-0493(2002)130<2110:TEOVWS>2.0.CO;2).
- Corbosiero, K.L. and Molinari, J. (2003) The relationship between storm motion, vertical wind shear, and convective asymmetries in tropical cyclones. *Journal of the Atmospheric Sciences*, 60(2), 366–376. [https://doi.org/10.1175/1520-0469\(2003\)060<0366:TRBSMV>2.0.CO;2](https://doi.org/10.1175/1520-0469(2003)060<0366:TRBSMV>2.0.CO;2).
- Dai, A. (2006) Precipitation characteristics in eighteen coupled climate models. *Journal of Climate*, 19(18), 4605–4630. <https://doi.org/10.1175/JCLI3884.1>.
- Dee, D.P. and Uppala, S. (2009) Variational bias correction of satellite radiance data in the ERA-Interim reanalysis. *Quarterly Journal of the Royal Meteorological Society*, 135(644), 1830–1841. <https://doi.org/10.1002/qj.493>.
- Dong, M., Chen, L., Li, Y., Cheng, Z. and Zhen, P. (2013) Numerical study of cold air impact on rainfall reinforcement associated with tropical cyclone TALIM (2005): impact of different cold air intensity. *Journal of Tropical Meteorology*, 19(1), 87–96.
- Emanuel, K. (2003) Tropical cyclones. *Annual Review of Earth and Planetary Sciences*, 31(1), 75–104. <https://doi.org/10.1146/annurev.earth.31.1.00901.141259>.

- Emanuel, K. and Zhang, F. (2017) The role of inner-core moisture in tropical cyclone predictability and practical forecast skill. *Journal of the Atmospheric Sciences*, 74(7), 2315–2324. <https://doi.org/10.1175/JAS-D-17-0008.1>.
- Frank, W.M. and Ritchie, E.A. (1999) Effects of environmental flow upon tropical cyclone structure. *Monthly Weather Review*, 127(9), 2044–2061. [https://doi.org/10.1175/1520-0493\(1999\)127<2044:EOEFUT>2.0.CO;2](https://doi.org/10.1175/1520-0493(1999)127<2044:EOEFUT>2.0.CO;2).
- Frank, W.M. and Ritchie, E.A. (2001) Effects of vertical wind shear on the intensity and structure of numerically simulated hurricanes. *Monthly Weather Review*, 129(9), 2249–2269. [https://doi.org/10.1175/1520-0493\(2001\)129<2249:EOVWSO>2.0.CO;2](https://doi.org/10.1175/1520-0493(2001)129<2249:EOVWSO>2.0.CO;2).
- Fudeyasu, H., Iizuka, S. and Matsuura, T. (2006) Impact of ENSO on landfall characteristics of tropical cyclones over the western North Pacific during the summer monsoon season. *Geophysical Research Letters*, 33(21). <https://doi.org/10.1029/2006GL027449>.
- Hanley, D., Molinari, J. and Keyser, D. (2001) A composite study of the interactions between tropical cyclones and upper-tropospheric troughs. *Monthly Weather Review*, 129(10), 2570–2584. [https://doi.org/10.1175/1520-0493\(2001\)129<2570:ACSOTI>2.0.CO;2](https://doi.org/10.1175/1520-0493(2001)129<2570:ACSOTI>2.0.CO;2).
- Hong, C.-C., Li, Y.-H., Li, T. and Lee, M.-Y. (2011) Impacts of central Pacific and eastern Pacific El Niños on tropical cyclone tracks over the western North Pacific. *Geophysical Research Letters*, 38(16), L16712. <https://doi.org/10.1029/2011GL048821>.
- Hu, K., Huang, G., Zheng, X.-T., Xie, S.-P., Qu, X., Du, Y. and Liu, L. (2014) Interdecadal variations in ENSO influences on northwest Pacific–East Asian early summertime climate simulated in CMIP5 models. *Journal of Climate*, 27(15), 5982–5998. <https://doi.org/10.1175/JCLI-D-13-00268.1>.
- Huffman, G.J., Bolvin, D.T., Nelkin, E.J., Wolff, D.B., Adler, R.F., Gu, G. and Stocker, E.F. (2007) The TRMM multisatellite precipitation analysis (TMPA): quasi-global, multiyear, combined-sensor precipitation estimates at fine scales. *Journal of Hydrometeorology*, 8(1), 38–55. <https://doi.org/10.1175/JHM560.1>.
- Jiang, H., Halverson, J.B. and Simpson, J. (2008a) On the differences in storm rainfall from Hurricanes Isidore and Lili. Part I: satellite observations and rain potential. *Weather and Forecasting*, 23(1), 29–43. <https://doi.org/10.1175/2007WAF2005096.1>.
- Jiang, H., Halverson, J.B. and Zipser, E.J. (2008b) Influence of environmental moisture on TRMM-derived tropical cyclone precipitation over land and ocean. *Geophysical Research Letters*, 35(17), 179–190. <https://doi.org/10.1029/2008GL034658>.
- Jones, R.W. (1987) A simulation of hurricane landfall with a numerical model featuring latent heating by the resolvable scales. *Monthly Weather Review*, 115(10), 2279–2297. [https://doi.org/10.1175/1520-0493\(1987\)115<2279:ASOHLW>2.0.CO;2](https://doi.org/10.1175/1520-0493(1987)115<2279:ASOHLW>2.0.CO;2).
- Karori, M.A., Li, J. and Jin, F.-F. (2013) The asymmetric influence of the two types of El Niño and La Niña on summer rainfall over southeast China. *Journal of Climate*, 26(13), 4567–4582. <https://doi.org/10.1175/JCLI-D-12-00324.1>.
- Khouakhi, A., Villarini, G. and Vecchi, G.A. (2016) Contribution of tropical cyclones to rainfall at the global scale. *Journal of Climate*, 30(1), 359–372. <https://doi.org/10.1175/JCLI-D-16-0298.1>.
- Kimoto, M., Yasutomi, N., Yokoyama, C. and Emori, S. (2005) Projected changes in precipitation characteristics around Japan under the global warming. *SOLA*, 1, 85–88. <https://doi.org/10.2151/sola.2005-023>.
- Lau, N.-C. and Nath, M.J. (2000) Impact of ENSO on the variability of the Asian–Australian monsoons as simulated in GCM experiments. *Journal of Climate*, 13(24), 4287–4309. [https://doi.org/10.1175/1520-0442\(2000\)013<4287:IOEOTV>2.0.CO;2](https://doi.org/10.1175/1520-0442(2000)013<4287:IOEOTV>2.0.CO;2).
- Li, R.C.Y. and Zhou, W. (2012) Changes in western Pacific tropical cyclones associated with the El Niño–Southern Oscillation cycle. *Journal of Climate*, 25(17), 5864–5878. <https://doi.org/10.1175/JCLI-D-11-00430.1>.
- Li, X., Yang, S., Wang, H., Jia, X. and Kumar, A. (2013) A dynamical–statistical forecast model for the annual frequency of western Pacific tropical cyclones based on the NCEP climate forecast system version 2. *Journal of Geophysical Research: Atmospheres*, 118(21), 12061–12074. <https://doi.org/10.1002/2013JD020708>.
- Li, Q., Lan, H., Chan, J.C.L., Cao, C., Li, C. and Wang, X. (2015) An operational statistical scheme for tropical cyclone induced rainfall forecast. *Journal of Tropical Meteorology*, 21(2), 101–110. <https://doi.org/10.16555/j.1006-8775.2015.02.001>.
- Liu, K.S. and Chan, J.C.L. (2003) Climatological characteristics and seasonal forecasting of tropical cyclones making landfall along the South China Coast. *Monthly Weather Review*, 131(8), 1650–1662. <https://doi.org/10.1175/2554.1>.
- Liu, K.S., Chan, J.C.L., Cheng, W.C., Tai, S.L. and Wong, P.W. (2007) Distribution of convection associated with tropical cyclones making landfall along the South China Coast. *Meteorology and Atmospheric Physics*, 97(1), 57–68. <https://doi.org/10.1007/s00703-006-0244-1>.
- Lonfat, M., Marks, F.D. and Chen, S.S. (2004) Precipitation distribution in tropical cyclones using the Tropical Rainfall Measuring Mission (TRMM) microwave imager: a global perspective. *Monthly Weather Review*, 132(7), 1645–1660. [https://doi.org/10.1175/1520-0493\(2004\)132<1645:pditcu>2.0.CO;2](https://doi.org/10.1175/1520-0493(2004)132<1645:pditcu>2.0.CO;2).
- Marks, F.D. (1985) Evolution of the structure of precipitation in Hurricane Allen (1980). *Monthly Weather Review*, 113(6), 909–930. [https://doi.org/10.1175/1520-0493\(1985\)113<0909:EOTSOP>2.0.CO;2](https://doi.org/10.1175/1520-0493(1985)113<0909:EOTSOP>2.0.CO;2).
- Pfeifroth, U., Mueller, R. and Ahrens, B. (2012) Evaluation of satellite-based and reanalysis precipitation data in the tropical Pacific. *Journal of Applied Meteorology and Climatology*, 52(3), 634–644. <https://doi.org/10.1175/JAMC-D-12-049.1>.
- Qian, Y., Liang, C., Yuan, Z., Peng, S., Wu, J. and Wang, S. (2016) Upper-tropospheric environment–tropical cyclone interactions over the western North Pacific: a statistical study. *Advances in Atmospheric Sciences*, 33(5), 614–631. <https://doi.org/10.1007/s00376-015-5148-x>.
- Reichle, R.H., Liu, Q., Koster, R.D., Draper, C.S., Mahanama, S.P.P. and Partya, G.S. (2017) Land surface precipitation in MERRA-2. *Journal of Climate*, 30(5), 1643–1664. <https://doi.org/10.1175/JCLI-D-16-0570.1>.
- Rios Gaona, M.F., Villarini, G., Zhang, W. and Vecchi, G.A. (2018) The added value of IMERG in characterizing rainfall in tropical cyclones. *Atmospheric Research*, 209, 95–102. <https://doi.org/10.1016/j.atmosres.2018.03.008>.
- Rodgers, E.B., Chang, S.W. and Pierce, H.F. (1994) A satellite observational and numerical study of precipitation characteristics in western North Atlantic tropical cyclones. *Journal of Applied Meteorology*, 33(2), 129–139. [https://doi.org/10.1175/1520-0450\(1994\)033<0129:asoans>2.0.CO;2](https://doi.org/10.1175/1520-0450(1994)033<0129:asoans>2.0.CO;2).
- Rogers, R., Chen, S., Tenerelli, J. and Willoughby, H. (2003) A numerical study of the impact of vertical shear on the distribution of rainfall in Hurricane Bonnie (1998). *Monthly Weather Review*, 131(8), 1577–1599. <https://doi.org/10.1175/2546.1>.
- Saunders, M.A., Chandler, R.E., Merchant, C.J. and Roberts, F.P. (2000) Atlantic hurricanes and NW Pacific typhoons: ENSO spatial impacts on occurrence and landfall. *Geophysical Research Letters*, 27(8), 1147–1150. <https://doi.org/10.1029/1999GL010948>.
- Shapiro, L.J. (1983) The asymmetric boundary layer flow under a translating hurricane. *Journal of the Atmospheric Sciences*, 40(8), 1984–1998. [https://doi.org/10.1175/1520-0469\(1983\)040<1984:TABLEFU>2.0.CO;2](https://doi.org/10.1175/1520-0469(1983)040<1984:TABLEFU>2.0.CO;2).
- Shen, Y., Xiong, A., Wang, Y. and Xie, P. (2010) Performance of high-resolution satellite precipitation products over China. *Journal of Geophysical Research: Atmospheres*, 115(D2), D02114. <https://doi.org/10.1029/2009JD012097>.
- Sun, Y., Solomon, S., Dai, A. and Portmann, R.W. (2006) How often does it rain? *Journal of Climate*, 19(6), 916–934. <https://doi.org/10.1175/jcli3672.1>.
- Tuleya, R.E. and Kurihara, Y. (1978) A numerical simulation of the landfall of tropical cyclones. *Journal of the Atmospheric Sciences*, 35(2), 242–257. [https://doi.org/10.1175/1520-0469\(1978\)035<0242:ansotl>2.0.CO;2](https://doi.org/10.1175/1520-0469(1978)035<0242:ansotl>2.0.CO;2).
- Ueno, M. (2007) Observational analysis and numerical evaluation of the effects of vertical wind shear on the rainfall asymmetry in the typhoon inner-core region. *Journal of the Meteorological Society of Japan, Series II*, 85(2), 115–136. <https://doi.org/10.2151/jmsj.85.115>.
- Wang, B. and Chan, J.C.L. (2002) How strong ENSO events affect tropical storm activity over the western North Pacific. *Journal of Climate*, 15(13), 1643–1658. [https://doi.org/10.1175/1520-0442\(2002\)015<1643:HSEAT>2.0.CO;2](https://doi.org/10.1175/1520-0442(2002)015<1643:HSEAT>2.0.CO;2).
- Wang, B., Wu, R. and Fu, X. (2000) Pacific–East Asian teleconnection: how does ENSO affect East Asian climate? *Journal of Climate*, 13(9), 1517–1536. [https://doi.org/10.1175/1520-0442\(2000\)013<1517:PEATHD>2.0.CO;2](https://doi.org/10.1175/1520-0442(2000)013<1517:PEATHD>2.0.CO;2).
- Wang, B., Wu, R. and Li, T. (2003) Atmosphere–warm ocean interaction and its impacts on Asian–Australian monsoon variation. *Journal of Climate*, 16(8), 1195–1211. [https://doi.org/10.1175/1520-0442\(2003\)16<1195:AIOAII>2.0.CO;2](https://doi.org/10.1175/1520-0442(2003)16<1195:AIOAII>2.0.CO;2).
- Wen, G., Liu, C., Bi, X. and Huang, H. (2017) A composite study of asymmetries of tropical cyclones after making landfall in Guangdong province.

- Journal of Tropical Meteorology*, 23(4), 417–425. <https://doi.org/10.16555/j.1006-8775.2017.04.007>.
- Wingo, M.T. and Cecil, D.J. (2009) Effects of vertical wind shear on tropical cyclone precipitation. *Monthly Weather Review*, 138(3), 645–662. <https://doi.org/10.1175/2009MWR2921.1>.
- Wu, G. and Lau, N.-C. (1992) A GCM simulation of the relationship between tropical-storm formation and ENSO. *Monthly Weather Review*, 120(6), 958–977. [https://doi.org/10.1175/1520-0493\(1992\)120<0958:AGSOTR>2.0.CO;2](https://doi.org/10.1175/1520-0493(1992)120<0958:AGSOTR>2.0.CO;2).
- Wu, M. C., Chang, W. L. and Leung, W. M. (2004) Impacts of El Niño–Southern Oscillation events on tropical cyclone landfalling activity in the Western North Pacific. *Journal of Climate*, 17(6), 1419–1428. [https://doi.org/10.1175/1520-0442\(2004\)017<1419:IOENOE>2.0.CO;2](https://doi.org/10.1175/1520-0442(2004)017<1419:IOENOE>2.0.CO;2).
- Wu, R., Hu, Z.-Z. and Kirtman, B.P. (2003) Evolution of ENSO-related rainfall anomalies in East Asia. *Journal of Climate*, 16(22), 3742–3758. [https://doi.org/10.1175/1520-0442\(2003\)016<3742:EOERA1>2.0.CO;2](https://doi.org/10.1175/1520-0442(2003)016<3742:EOERA1>2.0.CO;2).
- Wu, B., Li, T. and Zhou, T. (2010) Asymmetry of atmospheric circulation anomalies over the western North Pacific between El Niño and La Niña. *Journal of Climate*, 23(18), 4807–4822. <https://doi.org/10.1175/2010JCLI3222.1>.
- Xu, W., Jiang, H. and Kang, X. (2014) Rainfall asymmetries of tropical cyclones prior to, during, and after making landfall in south China and southeast United States. *Atmospheric Research*, 139(6), 18–26. <https://doi.org/10.1016/j.atmosres.2013.12.015>.
- Yonekura, E. and Hall, T.M. (2014) ENSO effect on East Asian tropical cyclone landfall via changes in tracks and genesis in a statistical model. *Journal of Applied Meteorology and Climatology*, 53(2), 406–420. <https://doi.org/10.1175/JAMC-D-12-0240.1>.
- Yu, Z., Ni, D., Gao, S., Min, J. and Ren, H. (2008) A numerical study of the severe heavy rainfall associated with Typhoon Haitang (2005). *Acta Meteorologica Sinica*, 22(2), 224–238. <https://doi.org/10.1029/2007JD008874>.
- Yu, Z., Yu, H., Chen, P., Qian, C. and Yue, C. (2009) Verification of tropical cyclone-related satellite precipitation estimates in mainland China. *Journal of Applied Meteorology and Climatology*, 48(11), 2227–2241. <https://doi.org/10.1175/2009JAMC2143.1>.
- Yu, Z., Wang, Y. and Xu, H. (2015) Observed rainfall asymmetry in tropical cyclones making landfall over China. *Journal of Applied Meteorology and Climatology*, 54(1), 117–136. <https://doi.org/10.1175/jamc-d-13-0359.1>.
- Yuan, J., Zhou, W., Huang, H. and Liao, F. (2010) Observational analysis of asymmetric distribution of convection associated with tropical cyclones “CHANCHU” and “PRAPIROON” making landfall along the South China Coast. *Journal of Tropical Meteorology*, 16(2), 171–180. <https://doi.org/10.3969/j.issn.1006-8775.2010.02.009>.
- Zhang, F., Weng, Y., Kuo, Y.-H., Whitaker, J.S. and Xie, B. (2010) Predicting typhoon Morakot’s catastrophic rainfall with a convection-permitting mesoscale ensemble system. *Weather and Forecasting*, 25(6), 1816–1825. <https://doi.org/10.1175/2010WAF2222414.1>.
- Zhang, W., Graf, H.F., Leung, Y. and Herzog, M. (2012) Different El Niño types and tropical cyclone landfall in East Asia. *Journal of Climate*, 25(19), 6510–6523. <https://doi.org/10.1175/JCLI-D-11-00488.1>.
- Zhang, W., Leung, Y. and Fraedrich, K. (2015) Different El Niño types and intense typhoons in the western North Pacific. *Climate Dynamics*, 44(11), 2965–2977. <https://doi.org/10.1007/s00382-014-2446-4>.
- Zhang, W., Vecchi, G.A., Villarini, G., Murakami, H., Gudgel, R. and Yang, X. (2016) Statistical–dynamical seasonal forecast of western North Pacific and East Asia landfalling tropical cyclones using the GFDL FLOR coupled climate model. *Journal of Climate*, 30(6), 2209–2232. <https://doi.org/10.1175/JCLI-D-16-0487.1>.
- Zhang, Q., Gu, X., Li, J., Shi, P. and Singh, V.P. (2017) The impact of tropical cyclones on extreme precipitation over coastal and inland areas of China and its association to ENSO. *Journal of Climate*, 31(5), 1865–1880. <https://doi.org/10.1175/JCLI-D-17-0474.1>.
- Zhang, Q., Lai, Y., Gu, X., Shi, P. and Singh, V.P. (2018) Tropical cyclonic rainfall in China: changing properties, seasonality, and causes. *Journal of Geophysical Research: Atmospheres*, 123(9), 4476–4489. <https://doi.org/10.1029/2017JD028119>.
- Zhao, T. and Yatagai, A. (2014) Evaluation of TRMM 3B42 product using a new gauge-based analysis of daily precipitation over China. *International Journal of Climatology*, 34(8), 2749–2762. <https://doi.org/10.1002/joc.3872>.
- Zhou, C. and Wang, K. (2017) Contrasting daytime and nighttime precipitation variability between observations and eight reanalysis products from 1979 to 2014 in China. *Journal of Climate*, 30(16), 6443–6464. <https://doi.org/10.1175/JCLI-D-16-0702.1>.
- Zhu, L., Wan, Q., Shen, X., Meng, Z., Zhang, F., Weng, Y., Sippel, J., Gao, Y., Zhang, Y. and Yue, J. (2015) Prediction and predictability of high-impact western Pacific landfalling tropical cyclone Vicente (2012) through convection-permitting ensemble assimilation of Doppler radar velocity. *Monthly Weather Review*, 144(1), 21–43. <https://doi.org/10.1175/MWR-D-14-00403.1>.

**How to cite this article:** Wen G, Huang G, Huang H, Liu C, Bi X. Observed rainfall asymmetry of tropical cyclone in the process of making landfall in Guangdong, south China. *Int J Climatol*. 2019;39: 3379–3395. <https://doi.org/10.1002/joc.6027>